



# Integrating susceptibility maps of multiple hazards and building exposure distribution: a case study of wildfires and floods for the province of Quang Nam, Vietnam

Chinh Luu<sup>1</sup>, Giuseppe Forino<sup>2</sup>, Lynda Yorke<sup>3</sup>, Hang Ha<sup>4</sup>, Quynh Duy Bui<sup>4</sup>, Hanh Hong Tran<sup>5</sup>, Dinh Quoc Nguyen<sup>6</sup>, Hieu Cong Duong<sup>7</sup>, and Matthieu Kervyn<sup>8</sup>

<sup>1</sup>Faculty of Hydraulic Engineering, Hanoi University of Civil Engineering, Hanoi, 100000, Vietnam

<sup>2</sup>School of Science, Engineering & Environment, University of Salford, Manchester, M5 4WT, UK

<sup>3</sup>School of Environmental and Natural Sciences, Bangor University, Bangor, Gwynedd, LL57 2DG, UK

<sup>4</sup>Department of Geodesy, Hanoi University of Civil Engineering, Hanoi, 100000, Vietnam

<sup>5</sup>Faculty of Geomatics and Land Administration, Hanoi University of Mining and Geology, Hanoi, 100000, Vietnam

<sup>6</sup>Environmental Chemistry and Ecotoxicology Lab, Phenikaa University, Hanoi, 12116, Vietnam

<sup>7</sup>Institute of Geodesy Engineering Technology, Hanoi University of Civil Engineering, Hanoi, 100000, Vietnam

<sup>8</sup>Department of Geography, Vrije Universiteit Brussel, Brussels, 1050, Belgium

**Correspondence:** Chinh Luu (chinhlt@huce.edu.vn)

Received: 9 January 2024 – Discussion started: 29 January 2024

Revised: 15 September 2024 – Accepted: 7 October 2024 – Published: 5 December 2024

**Abstract.** Natural hazards have serious impacts worldwide on society, economy, and environment. In Vietnam, throughout the years, natural hazards have caused significant loss of lives as well as severe devastation to houses, crops, and transportation. This research presents a new approach to multi-hazard (floods and wildfires) exposure estimates using machine learning models, Google Earth Engine, and spatial analysis tools for a typical case study in the province of Quang Nam in Central Vietnam. A geospatial database is built for multiple-hazard modeling, including an inventory of climate-related hazards (floods and wildfires), topography, geology, hydrology, climate features (temperature, rainfall, wind), land use, and building data for exposure assessment. The susceptibility of each hazard is first modeled and then integrated into a multi-hazard exposure matrix to demonstrate a hazard profiling approach to multi-hazard risk assessment. The results are explicitly illustrated for flood and wildfire hazards and the exposure of buildings. Susceptibility models using the random forest approach provide model accuracy of AUC (area under the receiver operating characteristic curve) = 0.882 and 0.884 for floods and wildfires, respectively. The flood and wildfire hazards are combined within a semi-quantitative matrix to assess the building exposure

to different hazards. Digital multi-hazard exposure maps of floods and wildfires aid the identification of areas exposed to climate-related hazards and the potential impacts of hazards. This approach can be used to inform communities and regulatory authorities on where to develop and implement long-term adaptation solutions.

## 1 Introduction

Different geographic areas worldwide, including mountainous, delta, and coastal regions, are facing distinct hazards and combinations of hazards (Rentschler et al., 2022). These challenges are intensified by population growth, urbanization, globalization, and climate change-induced shifts in extreme weather patterns, amplifying their adverse effects (Khatakho et al., 2021; Bangalore et al., 2018). While floods and storms represent the main hazards affecting Asian countries, risks from other hazards, such as landslides and wildfires, are also exacerbated by more extreme climate patterns, land use changes, and population expansion in these nations (IPCC, 2022). People who depend on natural resources lose

their livelihoods and become more vulnerable (Balica et al., 2015).

Due to its geographical location and unique natural conditions, Vietnam is exposed to various natural hazards: floods, landslides, droughts, and wildfires, which are further exacerbated by human activities combined with extreme weather conditions (Gan et al., 2021). The central region of Vietnam, particularly the province of Quang Nam, is highly vulnerable to natural hazards, making sustainable development tasks very challenging (Nguyen et al., 2023). Floods associated with tropical storms during the monsoon season (Luu et al., 2021) and wildfires exacerbated by dry seasons and high temperatures pose frequent threats and require comprehensive assessments of multi-hazard susceptibility and exposure in Quang Nam (Du et al., 2018). The impacts of these natural hazards hinder local development initiatives and exacerbate socioeconomic disparities (Khan et al., 2020). Disrupted agricultural activities, damaged infrastructure, and compromised access to essential services hinder the region's progress, while the loss of lives and properties deepens the social and economic burdens (Skilodimou et al., 2019). Notwithstanding these long-standing issues with floods and wildfires in the province of Quang Nam in Vietnam, limited studies have focused on multi-hazard susceptibility and exposure assessments.

The province of Quang Nam is characterized by a coastal region with low-lying topography, facing high flood risks due to heavy rainfall, typhoons, and potential breaches of dams and levees (Chau et al., 2014). The province has two large river catchments: the Vu Gia–Thu Bon and Tam Ky rivers. Away from the coast, the province is characterized by steep terrains and a dense river network. The prolonged heavy rainfall of the monsoon season in this dissected landscape results in yearly riverine floods in the lowland area and along the coast. This issue holds particular significance for the province of Quang Nam because flood events pose a direct threat to human lives and cause significant damage to its infrastructure, education, economic development, and health-related services (Lee et al., 2020).

Wildfires are also a natural hazard with devastating consequences, posing a severe threat to the environment and human communities (Tedim et al., 2015). Wildfires often occur due to a complex interplay of dry weather conditions, high temperatures, low humidity, flammable vegetation, and other geoenvironmental factors (Kalantar et al., 2020). Vietnam is particularly prone to fire events, especially in the northern part (Trang et al., 2022) and the central region (Nguyen et al., 2023). According to the statistical data from the Global Forest Watch, Vietnam has had a total of 674 612 wildfire alerts since 2012 and has ranked sixth in Southeast Asia regarding wildfires in the last 2 decades (Ansori, 2021).

The term “multi-hazard” refers to the fact that hazards often interact in complex ways, and their combined impact might be greater than the sum of individual hazards (Wing et al., 2018). The dynamic interplay between flood probabil-

ity in wet seasons and wildfire likelihood in dry seasons can be influenced by various factors, including environmental conditions, climatic patterns, topography, vegetation cover, and land use patterns (Skilodimou et al., 2021; Bountzouklis et al., 2022). Wildfires can significantly impact landscape hydrology by destroying vegetation cover and disrupting soil structure, reducing infiltration rates and heightening surface runoff during subsequent rain events (Mueller et al., 2018). Floods can reduce the formation and expansion of wildfire risks by wetting vegetation and soil, temporarily mitigating the likelihood of ignition and fire spread (Papaioannou et al., 2023). However, flood events can disrupt natural drainage patterns, saturate soils, and promote vegetation development, fueling wildfires in dry seasons (Eisenbies et al., 2007). In general, the formation of multi-hazard events often results from dynamic spatial and temporal interactions among various factors (De Angeli et al., 2022); significantly, floods and wildfires can exacerbate or mitigate each other's impacts depending on seasonal fluctuations, environmental conditions, or extreme climatic variability (Yu et al., 2023). Broadening the assessment framework for these spatial and dynamic interactions can lead to a more comprehensive and accurate risk evaluation (De Angeli et al., 2022). Thus, multi-hazard susceptibility and exposure assessments are required for efficient disaster risk management (Zhou et al., 2015). Multi-hazard susceptibility assessment provides insights into the spatial co-occurrence of different hazard types (Rusk et al., 2022). Multi-hazard exposure assessment enables the evaluation of the potential impact of multi-hazards on people, buildings, and critical facilities, which supports disaster management activities (De Angeli et al., 2022).

Advanced technologies, such as machine learning (ML), remote sensing, and big data analytics, play a critical role in predicting, monitoring, and mitigating the impact of hazards (Velev and Zlateva, 2023). Currently, Google Earth Engine (GEE), a cloud-based geospatial processing platform developed by Google in 2010, offers an extensive and up-to-date archive of satellite imagery, robust analysis tools, custom ML algorithm development, and the capacity to integrate multiple data sources (Tamiminia et al., 2020).

Various studies have applied ML algorithms, including classification and regression trees (CART) and random forest (RF), in modeling natural hazard susceptibility and have proven the high performance and accuracy of these models (Chen et al., 2018; Kim et al., 2017). CART and RF have been used to build susceptibility maps for single hazards, e.g., forest fires (Pourtaghi et al., 2016) or landslides (Wu et al., 2022); to develop the multi-hazard (forest fires and droughts) susceptibility maps for the Gangwon-do region in South Korea (Piao et al., 2022); and to construct multi-hazard (flood, landslides, forest fire, and earthquake) susceptibility maps in Khuzestan Province, Iran (Pourghasemi et al., 2023). Most of these studies have indicated that ML models perform well in estimating multi-hazard susceptibility but have not mentioned multi-hazard exposure assessment. Meanwhile,

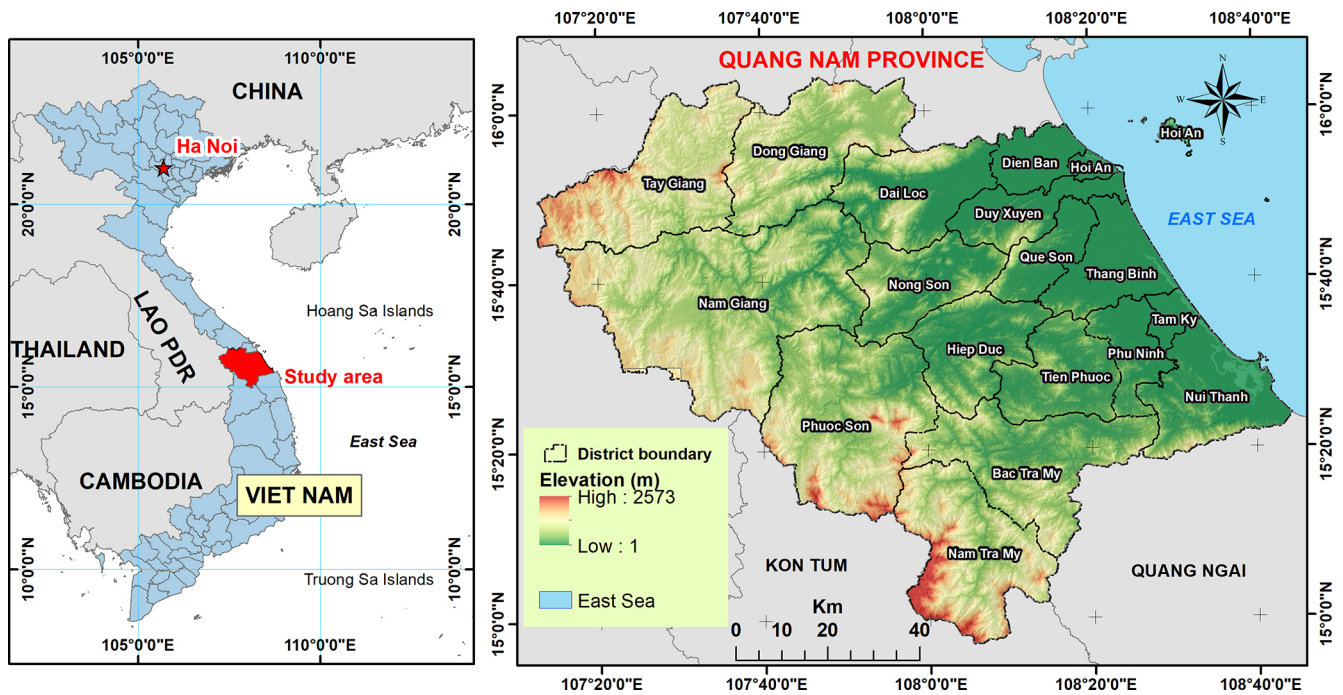


**Figure 1.** Elevation map of the study area: the province of Quang Nam in Vietnam (source: Shuttle Radar Topographic Mission digital elevation model).

multi-hazard exposure assessment can help recognize overlapping exposures and comprehend the intricate relationships between several hazards (Wang et al., 2020).

Therefore, the study aims are (i) to present and apply a methodological approach to assess and map susceptibility of multiple hazards for the province of Quang Nam; (ii) to utilize two ML models, CART and RF, that have been implemented on the GEE platform to build the susceptibility maps of flood and wildfire hazards for the province of Quang Nam; and (iii) to integrate the hazard-specific susceptibility maps with built-environment data to assess the multi-hazard exposure.

## 2 Study area

The province of Quang Nam is located in the central region of Vietnam, which has significant economic growth and huge tourism potential. Since the “economic reforms” and opening to foreign investment in 1986, the province of Quang Nam has seen significant socioeconomic transformations, such as the development of industrial zones and tourism. However, this fast development presents several issues for the province in pursuing sustainable development, necessitating optimal use of natural and sociocultural resources (Chau et al., 2014). Quang Nam had a total population of 1.84 million in 2019, with over 73 % of the population residing in the coastal plain, comprising just 25 % of the total geographical area. The Kinh ethnic group comprises 92.3 % of the population; the

remainder consists of many ethnic minorities, including the Co Tu, Xo Dang, M’ong, Co, and Gie Trieng. Agriculture, forestry, and fisheries accounted for 56 % of the total labor force, although their contribution to the GDP is only 21.4 % (<https://quangnam.gov.vn/>, last access: 1 September 2024).

Quang Nam encompasses a large topographic gradient, from a coastal plain to steep mountains, with a total area of 10 438 km<sup>2</sup> (Fig. 1). The complex topography due to the Annamite Range leads to strong separation in climate conditions and landscape characteristics. Terrain elevation gradually lowers from west to east, with mountainous areas (slope of 15° or more) concentrated mainly in the west following the Annamite Range and the flood plains running along the coastline. The tropical monsoon climate is characterized by two distinct weather seasons in a year: the dry season from March to August, associated with water shortages, leading to droughts, and the rainy season from September to February, often bringing excess water and leading to floods. Quang Nam has the highest annual rainfall in Vietnam, averaging 2200 to 2700 mm, with 70 % falling during the rainy season. The main hazards in the province of Quang Nam are floods, landslides, droughts, and wildfires (Du et al., 2018). This study focuses on assessing and mapping flood and wildfire hazards in the province.

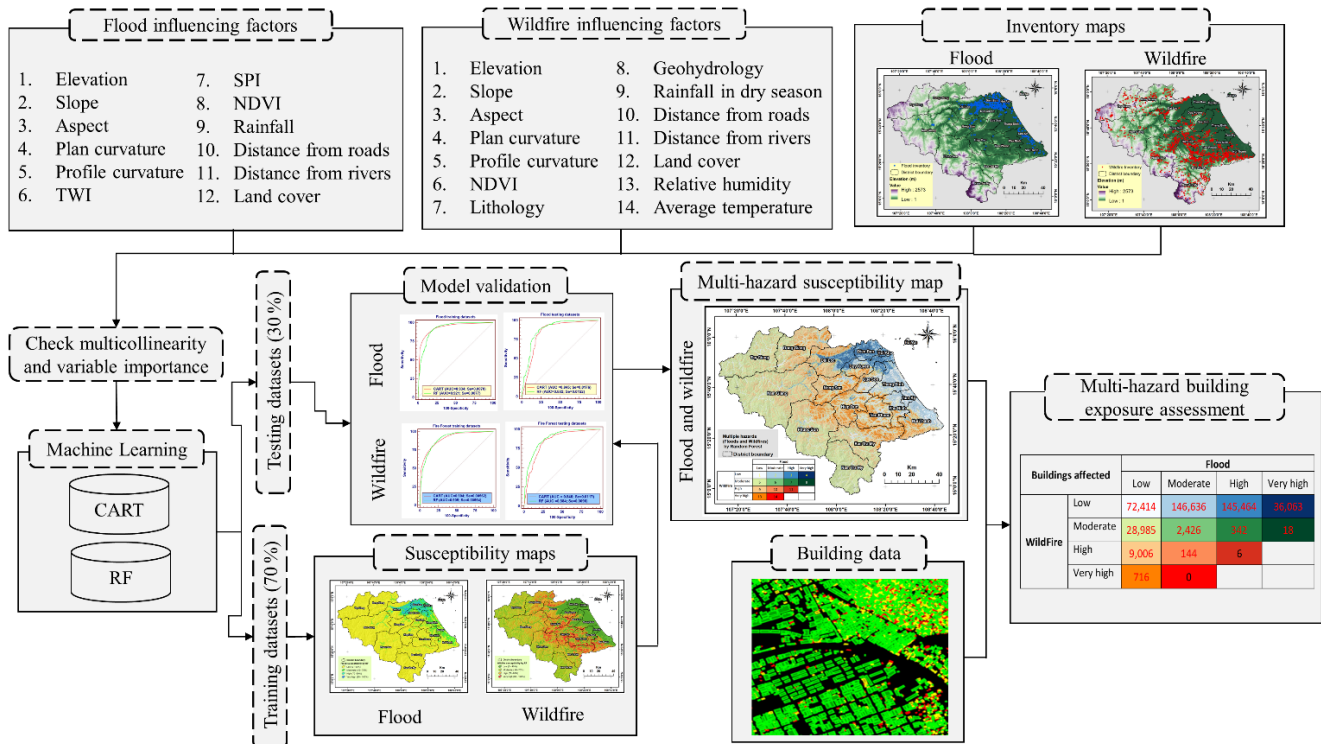


**Figure 2.** Methodology flowchart for multi-hazard exposure assessment and mapping in this study.

### 3 Methodology

#### 3.1 Methodology flowchart

The multi-hazard exposure assessment process comprises seven main stages:

1. Inventory maps of each hazard were created based on historical data collection.
2. Factors potentially influencing the spatial distribution of floods and wildfires were collected, including topography, geology, hydrology, climate (temperature, wetness, wind), and land use based on their relevance and data availability (Luu et al., 2018).
3. The influencing factors of each hazard were tested for multicollinearity to enhance the reliability and stability of the model's predictions.
4. CART and RF models were developed on the GEE cloud computing platform to construct susceptibility maps of floods and wildfires separately.
5. The area under the ROC (receiver operating characteristic) curve (hereafter, AUC) was utilized to assess the predictive performance of the susceptibility maps to choose the best model for each hazard and validate it.

6. The flood susceptibility map and the wildfire susceptibility map were combined to build a susceptibility map for multi-hazard co-occurrence.

7. This multi-hazard susceptibility map was overlaid with the building data to create a multi-hazard exposure map for the study area (Fig. 2).

#### 3.2 Data used

##### 3.2.1 Inventories of floods and wildfires

Developing accurate hazard inventories is crucial for susceptibility mapping (Bui et al., 2023a). In this study, the flood marker points recorded for all flood events from 2007 to 2023 were considered, as reported by the Quang Nam Provincial Steering Committee of Natural Disaster Prevention and Control. We removed duplicate flood points. A total of 847 historical flood marks were obtained from this database — these correspond mainly to the 2007, 2009, and 2013 flood events with the largest spatial extent. Each flood mark comprises a unique identifier, geographical coordinates (longitude and latitude), flood depth, and provider information. A second source of information was derived from mapping flood extent on synthetic aperture radar data from Sentinel 1 for 2017 to 2023, which we compare with official reports from the provincial committee. The flood detection algorithm described in Mai Sy et al. (2023) was implemented in Google

Earth Engine. Inundation areas detected on the different Sentinel 1 scenes were overlaid and compared with the flood mark locations to avoid duplicates. A total of 47 new flood sites were detected and integrated as additional points (using the centroid of the flood site), with 847 historical flood marks for the inventory data.

The final flood inventory includes 894 flood locations: 70 % of them (626 locations) were randomly selected to calibrate the flood susceptibility model, and the remaining 30 % (268 locations) were designated for validating purposes (Fig. 3). In addition, 894 non-flood locations were randomly selected across the study area using the “create random point tool” in ArcGIS software. Non-flood points were chosen only in zones outside the flood-affected zones in our inventory. Additionally, we excluded steep slopes ( $> 10^\circ$ ) or areas of positive relief (such as hilltops) from the selection of non-flood points, as these locations that cannot be associated with floods would artificially increase the accuracy of the susceptibility model. The non-flood points were then classified in a ratio of 70/30, mirroring the classification of the flood locations. This process was undertaken to create a comprehensive database for input into the GEE platform, which was utilized for modeling and validation.

For the wildfire inventory, this study involved the collection of 1911 wildfire locations recorded during the dry season (March to August) from 2020 to 2023 (Fig. 3) from the National Forest Protection Department’s website (available at <https://watch.pcccr.vn/thongKe/diemChay>, last access: 1 September 2024). This agency utilizes data from many satellites (Aqua, J1, Suomi, and Terra) that are regularly received at the TerraScan receiving station located at the National Forest Protection Department. The use of near-infrared bands from many satellites helps to identify the presence of heat associated with active wildfires on the ground (Giglio et al., 2008). The website database was checked and filtered to avoid duplicated wildfire locations, dates, and commune data field conditions. The wildfire location data (points) represent the specific fire sites captured by one type of satellite inside a particular commune at a given time. We filtered the database of the National Forest Protection Department to retain only wildfire spots exceeding a minimum size threshold of 2 ha, as smaller fire areas should be considered human-induced. To determine the non-fire points, we randomly selected points within the zones with forested and natural vegetation land cover, which were not identified as wildfires in the inventory. We excluded residential areas, water, and crop areas from the selection of non-fire points, as these cannot be associated with wildfires corresponding to the criteria selected in this study and would artificially increase the accuracy of our susceptibility model.

### 3.2.2 Influencing factors

Several factors significantly influence flood and wildfire occurrences. Low-lying areas are prone to flooding, while el-

evated regions can hinder fires (Pourtaghi et al., 2016; Bui et al., 2023a). Slope, slope aspect, and curvature affect water flow, erosion, and fire spread, with steeper slopes mitigating or accelerating these hazards (Dottori et al., 2018; Trang et al., 2022). The topographic wetness index (TWI) and stream power index (SPI) help quantify water accumulation and erosion risks. Vegetation density, assessed using the normalized difference vegetation index (NDVI), impacts both flood absorption and fire fuel availability (Abedi Gheshlaghi et al., 2021; Gonzalez-Arqueros et al., 2018). Road and river proximity also influence flood and fire dynamics, while land cover, lithology, and geohydrology influence water retention and fire susceptibility (Ha et al., 2023; Hosseini and Lim, 2022). Rainfall patterns and temperatures, particularly during dry seasons, further contribute to both flood and wildfire risks (Abram et al., 2021; Ahmadlou et al., 2018). These factors are modeled using data from satellite imagery, DEMs, and long-term climate records (in Appendix A).

### 3.2.3 Built-environment data

In this study, we use the building data to assess the potential impact of flood and wildfire hazards on building infrastructure, considering housing/building a key livelihood asset. Spatial data on the building infrastructure of the province of Quang Nam are extracted from the Open Buildings dataset of Google ([https://developers.google.com/earth-engine/datasets/catalog/GOOGLE\\_Research\\_open-buildings\\_v3\\_polygons](https://developers.google.com/earth-engine/datasets/catalog/GOOGLE_Research_open-buildings_v3_polygons), last access: 1 September 2024). The collection contains information about each building, including a polygon representation of its footprint on the ground and a confidence score showing the level of certainty about its classification as a building (Sirko et al., 2021). We filtered the data with a confidence level of more than 80 % and an area larger than 30 m for accurate data on buildings (assuming the minimum size for a residential building). The data are created by high-resolution satellite photography with a resolution of 50 cm. The selected data were checked visually against Google Earth and were shown to represent the large majority of buildings properly.

This study focuses on buildings in terms of elements exposed to hazards, considering their importance as critical economic assets and reflections of population distribution (Askar et al., 2021). Buildings are essential components of community infrastructure, and damage to them may have big social and economic effects, making them a crucial exposure indicator for risk assessment (Carreño et al., 2007). In addition, buildings often accommodate individuals and vital services; thus, their exposure to hazards and susceptibility to damage directly control the possibility of human fatalities and disturbance to everyday activities. In terms of vulnerability, buildings are not equally at risk from all hazards; their susceptibility varies depending on the hazard type and the structural characteristics of the building, although vulnerabil-

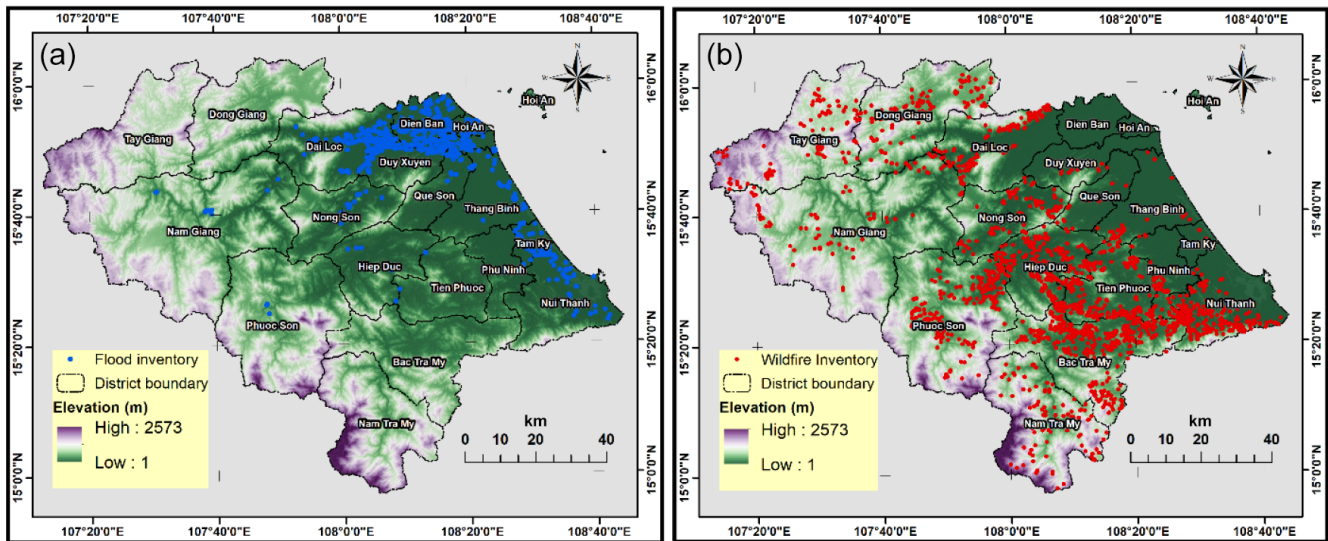


**Figure 3.** Inventory maps of flood (a) and wildfire (b) points in the province of Quang Nam.

ity is not considered explicitly in this study (Schneiderbauer and Ehrlich, 2004).

### 3.3 Methods

#### 3.3.1 Multicollinearity

The variance inflation factor (VIF) and tolerance values are critical statistical measures in detecting the presence of multicollinearity among input variables (Arabameri et al., 2018). The VIF values quantify how much the variance of an estimated regression coefficient increases due to multicollinearity (Ma et al., 2020). Tolerance is the reciprocal of VIF values and reflects the proportion of variance in a predictor that is not forecasted by a combination of other predictors (Bui et al., 2023b). Significant multicollinearity among input variables is detected if the VIF value surpasses 10 or the tolerance value drops below 0.1 (Miao et al., 2023). Variables found to be multicollinear will be deleted from the model, and the model will be run to check for multicollinearity again.

#### 3.3.2 Machine learning approach for hazard susceptibility modeling

This study has developed two ML models, including CART and RF, on the GEE workspace to construct hazard (flood and wildfire) susceptibility maps for the province of Quang Nam.

The CART was first introduced by Breiman et al. (1984). It is an algorithm used for both classification and regression tasks. CART builds binary trees recursively by splitting the dataset into subsets based on the feature values (Tang and Zhang, 2020). Mathematically, this algorithm can be summarized as follows (Ahmadlou et al., 2022):

1. A training dataset  $D = (Xs, Y)$  is inputted, where  $Xs$  denotes the feature variable and  $Y$  is the target variable (class labels for classification, numerical values for regression).
2. For the classification issue, the CART algorithm uses the Gini impurity coefficient on these subsets to measure the disorder or impurity of an input dataset. The Gini impurity coefficient is determined using the following equation:

$$\begin{aligned} \text{Gini}(D) &= \sum_{i=1}^J P_i(1 - P_i) = \sum_{i=1}^J P_i - \sum_{i=1}^J P_i^2 \\ &= 1 - \sum_{i=1}^J P_i^2, \end{aligned} \quad (1)$$

where  $\text{Gini}(D)$  is the Gini impurity coefficient of the input dataset  $D$ ,  $J$  represents the number of classes in the input dataset, and  $P_i$  denotes the probability of class  $i$  in dataset  $D$ .

The CART continues seeking the best feature and threshold recursively until a stopping criterion is met, such as maximum tree depth (*max\_depth*) or minimum samples in a leaf (*min\_samples\_leaf*). After that, the resulting tree can be used to classify new datasets.

Like all decision tree algorithms, CART is prone to overfitting, especially when the tree becomes too deep. To mitigate this, pruning techniques and hyperparameter tuning are often applied to optimize the tree's structure, ensuring generalizability to unseen data (Ahmadlou et al., 2022).

The RF is a widely used ML algorithm developed by Breiman (2001), which combines the output of multiple decision trees to reach a single result (Naghbi et al., 2016). It

is used for both classification and regression tasks (Genuer et al., 2010). The content of this technique can be described as follows (Breiman, 2001):

1. A training dataset  $D$  of  $N$  bootstrap samples  $D = (Xs, Y)$  is inputted, where  $Xs$  is the feature variable and  $Y$  is the target variable (class labels for classification, numerical values for regression). The RF technique creates multiple decision trees using bootstrapped subsets of the training data  $D$ . Each tree is constructed using  $N$  samples drawn with replacement (bootstrap sampling).
2. For each tree and at each split, a subset of features ( $m$ ) is randomly selected from the total number of features in the training dataset ( $M$ ) to ensure diversity among the trees.
3. Each tree in the RF algorithm is built using the selected bootstrap sample and features in the first and second steps. The tree is developed by recursively dividing the dataset based on the selected features and splitting criteria.
4. The RF technique combines these predictions (multiple decision trees) due to the specific tasks. The prediction mode from individual trees is the final classification task prediction.

### 3.3.3 Model validation and comparison

This study used the ROC curve and AUC to validate the predictive performance of each hazard susceptibility model, including CART and RF models. The ROC curve is generated by plotting the true-positive rate (sensitivity) against the false-positive rate ( $1 - \text{specificity}$ ) for different threshold values (Carter et al., 2016). Sensitivity quantifies the ability of the model to correctly identify susceptible areas, while specificity measures the capability to identify non-susceptible areas correctly (Meghanadh et al., 2022). The AUC is calculated to quantify the quality of the predictive model. The AUC values vary from 0 to 1, where AUC values of 0.5–0.6 reflect a low predictive performance, 0.7–0.8 is interpreted as a medium predictive performance, 0.8–0.9 indicates good predictive performance, and 0.9–1.0 denotes excellent predictive performance.

### 3.4 Experimental process

This study employed the GEE cloud computing platform for the pixel-based CART and RF algorithms to build susceptibility maps for flood and wildfire hazards separately. The input data were collected from various sources and formats. First, we pre-processed and converted these data into raster format with 30 m spatial resolution in a GIS environment.

Then, these data were uploaded into the GEE platform. Hyperparameter tuning technique was used to optimize the performance of ML algorithms, as they significantly affect the accuracy, efficiency, and generalization ability of ML models (Schratz et al., 2019). Various hyperparameter tuning methods include grid search, random search, gradient-based optimization, and Bayesian optimization. This hyperparameter tuning process of grid search was used for the modeling in this study, including the following steps:

- *Setup of the environment.* Install Python packages in the Google Earth Engine (GEE) application programming interface (API) to handle geospatial data and scikit-learn to develop ML models.
- *Data preparation.* Upload 15 landslide-affecting factors to the GEE environment to build the flood and wildfire susceptibility maps. The training and testing datasets have also been uploaded to this platform.
- *Hyperparameter tuning.* Use scikit-learn to develop various ML models (CART and RF) and define the hyperparameter search spaces for a grid search. This step involves setting reasonable value ranges for each hyperparameter in each model, for the CART model (*max\_Nodes*, *minLeafPopulation*) and the RF model (*numberOfTrees*, *bagFraction*, *seed*), described in Table 1. Then, scikit-optimize's grid search performs iterative assessments using the training data to select the hyperparameter combination that optimizes a chosen performance metric (ROC and AUC) on the testing data. The best hyperparameter combinations for each model are determined based on these performance metrics.
- *Model assessment.* Optionally, the final evaluation involves retraining the predictive models with the chosen hyperparameters on the training data. The performance of these retrained models is then assessed using the ROC curve and AUC value on the validation dataset to gauge their effectiveness.

## 4 Results

### 4.1 Assessment of multicollinearity and variable importance

In this research, the VIF and tolerance values of influencing factors for flood and wildfire susceptibility modeling are satisfactory, so all input factors are selected to develop hazard susceptibility maps (Table 2). In natural hazard susceptibility modeling, each input variable may influence the occurrences of each hazard in various ways (Pourghasemi et al., 2020). Variable importance assessment can identify which factors have the most significant impact on the hazard formations (Javidan et al., 2021). RF is one of the most popular ML algorithms for evaluating variable importance by measuring

**Table 1.** The hyperparameter values in the optimization process.

Model	Optimized hyperparameter	Explanation	Lower and upper limits	Optimal value
CART	<i>max_Nodes</i>	The maximum number of leaf nodes in each tree	2–500	150
	<i>minLeafPopulation</i>	Only create nodes whose training set contains at least this many points.	1–10	2
RF	<i>numberOfTrees</i>	The number of decision trees to create	100–1000	200
	<i>minLeafPopulation</i>	Only create nodes whose training set contains at least this many points	1–10	1
	<i>bagFraction</i>	The fraction of input to bag per tree	0.1–1.0	0.7
	<i>seed</i>	The randomization seed	0–42	23

**Table 2.** Assessment of multicollinearity and variable importance to flood-influencing factors.

Factors	Flood			
	Tolerance	VIF	Variable importance	Rank
Rainfall	0.832	1.225	0.1742	1
Distance from rivers	0.945	1.204	0.1620	2
NDVI	0.759	1.774	0.1330	3
Land use/land cover	0.582	2.160	0.1159	4
Aspect	0.98	1.019	0.1095	5
TWI	0.725	1.676	0.0753	6
Distance from roads	0.600	3.241	0.0709	7
Plan curvature	0.798	3.669	0.0695	8
Profile curvature	0.876	1.418	0.0320	9
Elevation	0.777	1.259	0.0300	10
Slope	0.748	2.106	0.0270	11
SPI	0.948	1.117	0.0007	12

how much they contribute to the model's accuracy (Fox et al., 2017). Thus, this technique was applied to assess the significance of all input variables. The results show that rainfall (weight = 0.1742), distance from rivers (weight = 0.1620), NDVI (weight = 0.1330), and land cover (weight = 0.1159) are the indicators that significantly contribute to the control of the spatial distribution of flood events within the study area.

The results presented in Table 3 demonstrate that temperature (weight = 0.1784), distance from rivers (weight = 0.1112), NDVI (weight = 0.1089), and distance from roads (weight = 0.1065) are the parameters that have a significant impact on the formation of wildfire events within the study area.

#### 4.2 Flood susceptibility map and model validation

For flood susceptibility models, the ROC curve analysis on the training dataset signifies that the CART model has the highest value of AUC (0.934), and the RF model has a lower AUC (0.921). The ROC curve analysis on the validation dataset reveals that the AUC value of the RF model (0.882)

**Table 3.** Assessment of multicollinearity and variable importance to wildfire-influencing factors.

Factors	Wildfire			
	Tolerance	VIF	Variable importance	Rank
Temperature	0.643	1.555	0.1784	1
Distance from rivers	0.697	1.435	0.1112	2
NDVI	0.835	1.198	0.1089	3
Distance from roads	0.472	2.118	0.1065	4
Slope	0.512	1.954	0.0953	5
Rainfall in dry season	0.384	2.603	0.0739	6
Land use/land cover	0.737	1.356	0.0613	7
Profile curvature	0.786	1.273	0.0538	8
Elevation	0.524	1.909	0.0500	9
Plan curvature	0.715	1.398	0.0481	10
Aspect	0.513	1.948	0.0473	11
Lithology	0.551	1.816	0.0420	12
Geohydrology	0.636	1.572	0.0233	13

is higher than that of the CART model (0.845). This result demonstrates that the RF model has the best predictive performance for flood susceptibility mapping (Fig. 4).

Since the RF shows good predictive performance, it is selected to generate the flood susceptibility map for the research area with the training dataset. The flood susceptibility map delineates the different geographical zones with increasing levels of susceptibility to flood events. We use the quantile method for classifying the susceptibility values with low (0%–40%), moderate (40–70%), high (70%–90%), and very high (90%–100%) classes and set the green–blue–yellow color scheme for flood susceptibility (Fig. 5). The high and very high susceptibility areas are along the main river and the coastal zone, consistent with the flood inventory shown in Fig. 3.

#### 4.3 Wildfire susceptibility map and model validation

The ROC curve analysis on the training dataset for wildfire susceptibility models denotes that both the CART and RF models have the same AUC value (0.905). In contrast, the

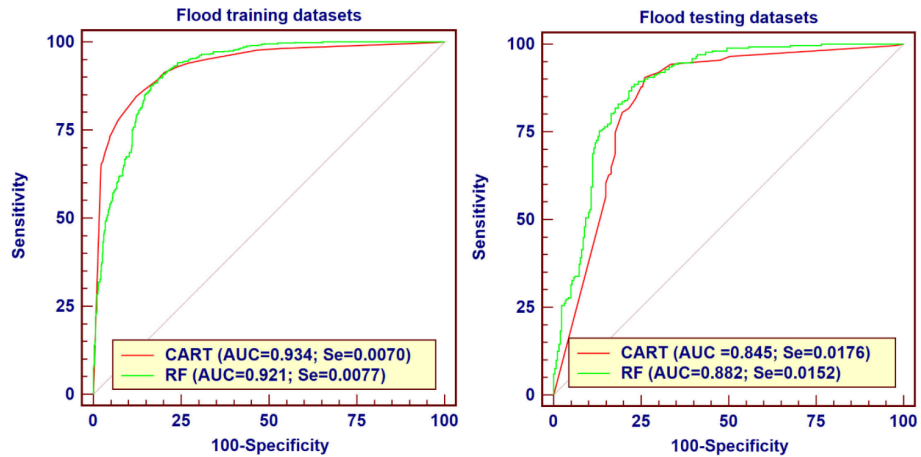


**Figure 4.** ROC curve and AUC analysis result from flood susceptibility modeling with training and validation datasets. Note: Se stands for standard error.

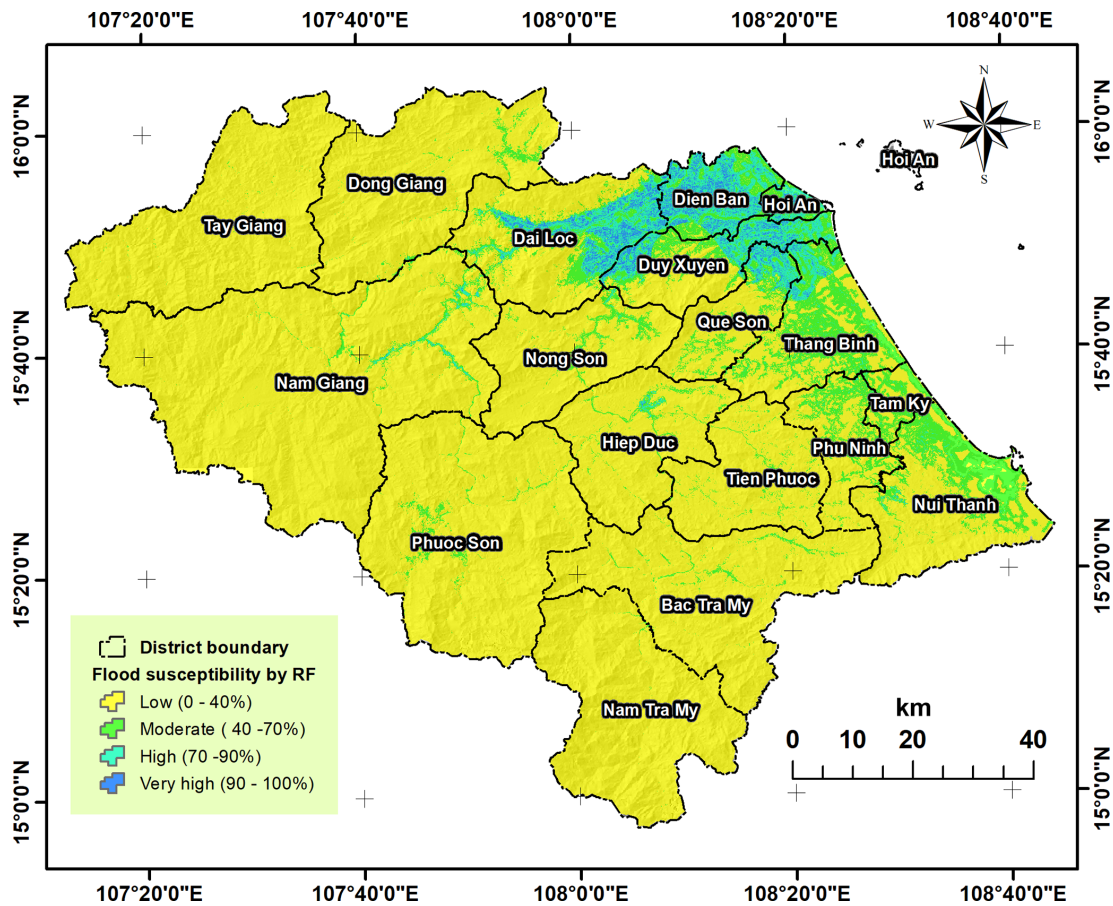


**Figure 5.** The flood susceptibility map derived using the RF model for the province of Quang Nam.

ROC curve analysis on the validation dataset reveals that the AUC value of the CART model (0.846) is lower than that of the RF model (0.884). This result reflects that the RF model is the best forecast model for wildfire susceptibility mapping (Fig. 6).

Given the satisfactory predictive performance shown by the RF model, it has been chosen as the preferred method for generating fire susceptibility maps for the study area using the provided training dataset. The wildfire susceptibility map demarcates the diverse levels of susceptibility to fire

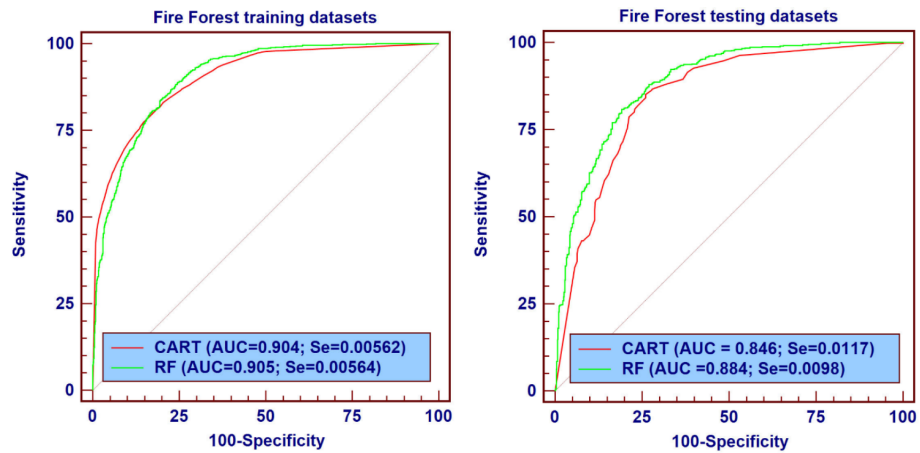


**Figure 6.** ROC curve and AUC analysis results from wildfire susceptibility modeling with training and testing datasets. Note: Se stands for standard error.

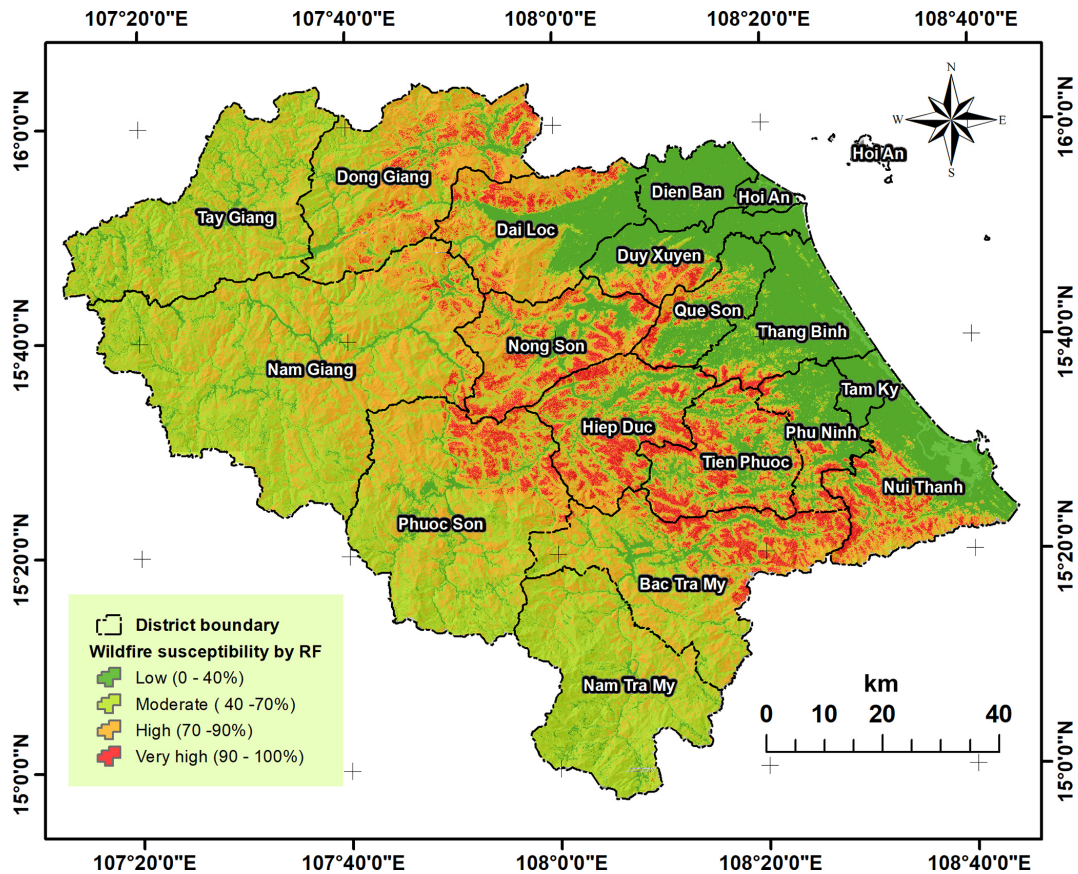


**Figure 7.** The wildfire susceptibility map was derived using the RF model for the province of Quang Nam.

occurrences. The same quantile approach is used to categorize susceptibility values. A green–yellow–red color scheme represents wildfire susceptibility (Fig. 7). The areas highly prone to wildfire hazards are in the mid-elevation areas, not the high mountainous or lowland areas, and agree with the wildfire distribution mapped in Fig. 3.

#### 4.4 Multi-hazard susceptibility and exposure mapping

The susceptibility map for hazard co-occurrence for the province of Quang Nam was generated by examining the spatial interplay between wildfires and floods. The map depicts a matrix-based classification that enables the definition

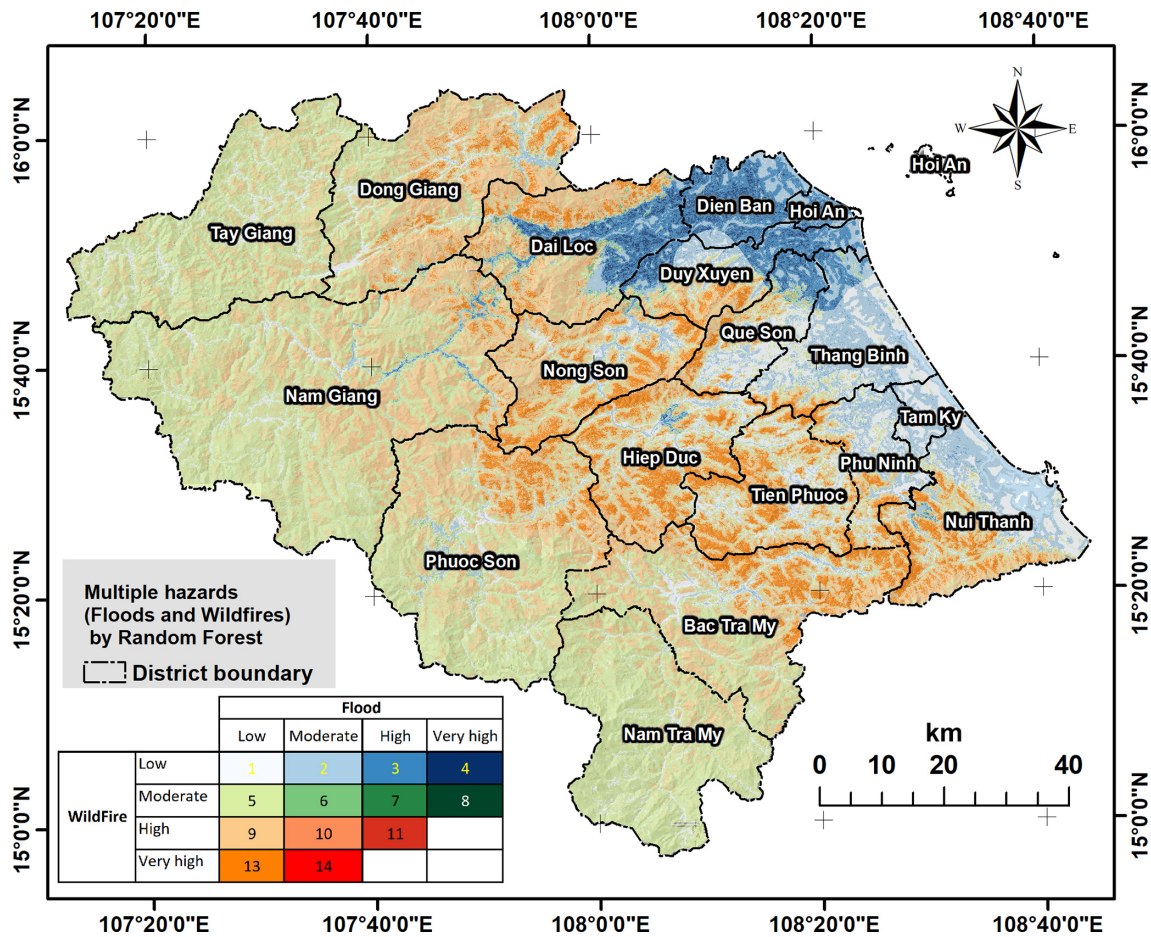


**Figure 8.** Integrated multi-hazard susceptibility classification combining floods and wildfires using the random forest algorithm for the province of Quang Nam.

of new susceptibility classes (low, moderate, high, very high) of combined hazards and provides a unique multi-hazard profile for each location (Fig. 8). In the matrix, not all combinations of hazards are represented, as there is no area with high susceptibility to floods and high susceptibility to wildfires. Combining the multi-hazards through a matrix gives a good visual overview of multi-hazards for the large scale of the whole province. The multi-hazard susceptibility map shows that the areas with very high wildfire susceptibility have low flood susceptibility and vice versa. The lowland coastal area is characterized by moderate to very high flood hazards but limited fire hazards (categories 2, 3, 4). The mid-altitude slopes are categorized by low flood but high to very high fire hazards (categories 9–10, 13), except for possible floods along the main valleys, and the upland slopes are associated with moderate to low levels of the two hazards (categories 1, 2, 5).

Our analysis examines the optimal sequence for integrating the two hazards, followed by assessing the exposure of buildings. The matrix of the number of buildings and area affected by each hazard level is converted into the percentage

of total buildings in each cell of multi-hazard levels. We can compare the two in Table 4. It is highlighted that the proportion of buildings in the category of very high flood and low fire susceptibility is much larger than the area of this category. In contrast, the proportion of buildings in category 13 (low flood and very high fire susceptibility) is much smaller than the area fraction. This highlights that measures to limit the impact on buildings (and so on people) to limit flood are much more important than for fire.

### 5 Discussion

Assessing susceptibility and exposure to several spatially co-occurring hazards is crucial and multifaceted in disaster management and community resilience (Menoni et al., 2012). In this study, floods and wildfires are examples of two hazards with different spatial patterns but quite similar spatial extent and frequency: assessment of the combined exposure to both hazards highlights that they have a very different impact on built-up infrastructure. Additional hazards, such as landslides or droughts, should be added to the scheme, with a multi-

**Table 4.** Statistics of the percentage of buildings affected and the percentage of area represented in each cell by flood and wildfire hazards in the province of Quang Nam.

Buildings affected (%)		Flood			
		Low	Moderate	High	Very high
WildFire	Low	16.375	33.159	32.894	8.155
	Moderate	6.554	0.549	0.077	0.004
	High	2.037	0.033	0.001	
	Very high	0.162	0		

Area affected (%)		Flood			
		Low	Moderate	High	Very high
WildFire	Low	9.605	8.353	3.920	1.010
	Moderate	38.587	0.559	0.021	0.000
	High	29.966	0.118	0.000	
	Very high	7.859	0.002		

dimension hazard matrix and profiling of each zone. This would help define the hazard profile for each zone and identify which areas are indeed affected by multiple and maybe combined hazards (Yousefi et al., 2020).

ML models have been extensively used in diverse hazard evaluations, such as flood, landslide, and wildfire susceptibility (Bui et al., 2023a; Ha et al., 2022; Pourtaghi et al., 2016). These techniques are advantageous in evaluating the efficacy of different models under comparable circumstances, considering similar influencing elements. This approach ensures a fair and unbiased determination of the most appropriate model for addressing a specific danger within a particular location. The modeling and mapping of multi-hazard susceptibility often rely on a system of multifaceted and multi-scaled natural factors, encompassing topography, geohydrology, environment, and hydrometeorology conditions within the research area (Tavakkoli Piralilou et al., 2022).

Our research analyzed the combined exposure of buildings to flood and wildfire hazards in the province of Quang Nam, Vietnam. Utilizing ML models (CART and RF) to assess the susceptibility of multiple hazards, we can show that the RF model exhibited comparable levels of accuracy for both flood and wildfire hazards. Additionally, both models demonstrated good performance for flood and wildfire susceptibility maps, aligning with earlier research findings (Hasanzadeh Nafari et al., 2016; Nachappa et al., 2020). The accuracy of a model is dependent on the selection of the influencing elements used in mapping natural hazard susceptibility (Pourtaghi et al., 2016). This study carefully checked multicollinearity for influential factors, and variable importance was measured to find the most suitable factors for the modeling input. In addition, the selection of the non-hazard points is also thoroughly carried out with the specific standards, contributing to better modeling performance.

The integration of the susceptibility maps of flood and wildfire hazards into a multi-hazard susceptibility matrix highlights that flood and wildfire events threaten different areas and proportions of the entire province of Quang Nam.

The multi-hazard map is built upon a susceptibility class matrix for flood and wildfire events instead of a simple summation of both susceptibility maps. Indeed, the matrix enables the identification of regions with different combinations of hazard susceptibility for floods and wildfires. The exposure maps generated by combining the susceptibility map with the built-environment data exhibit the total exposed housing for different susceptibility levels of each hazard and multi-hazards. Creating a multi-hazard exposure map that effectively delineates regions susceptible to floods and wildfires via the implementation of a matrix-based approach and combining the map with built-environment data to assess the exposure elements of the hazards has not previously been attempted by other researchers. The combination with exposure highlights that different districts have to deal with different combinations of hazard susceptibility and that exposure to fire is much lower than flood hazards despite the broad spatial distribution of the wildfire susceptibility. This combination is an important step towards an integrated risk assessment of spatially co-occurring hazards; however, the contrasted vulnerability of buildings relative to different hazards, taking into account the specific attributes of the building, is also important in controlling the potential damage (Šakić Trogljić et al., 2024). Such hazard-specific vulnerability functions for different building types still need to be constrained for the study area before a fully quantitative risk assessment can be completed.

Verifying multi-hazard exposure assessments is essential for ensuring the accuracy and reliability of the analysis, as well as for facilitating effective risk management strategies (Skilodimou et al., 2019). The multi-hazard exposure can be verified by analyzing historical damage data or examining the observed damage to vulnerable assets such as buildings, infrastructure, and natural resources (Khan et al., 2020). The 2020 flood and storm events caused 46 deaths; more than 117 000 properties to be flooded and damaged; and widespread damage to farmland, roads, irrigation works, and other infrastructure (VDMA, 2020). In addition, according to statistics from the Quang Nam Forest Protection Department, over the past 5 years in Quang Nam, there have been 136 forest fires that caused damage to more than 618 ha of various types of forests (available at <https://chicuckiemlam.snnptnt.quangnam.gov.vn/>, last access: 1 September 2024). These available statistics confirmed the larger exposure of buildings to floods than to wildfires, as highlighted in Table 4. However the lack of damage statistics per hazard type at a fine spatial resolution prevents the comparison of our multi-hazard exposure map with actual recorded damage.

Considering the spatial occurrence of hazards and the associated exposure to built-up environments enables highlighting which areas and which proportion of buildings are exposed to one specific hazard or both, which can be relevant for risk management. The consideration of temporal relationships between hazards (i.e., fire during the dry season inducing flood in the next rain season) or non-local dynamic inter-

actions (i.e., wildfire in upper catchment increasing flood occurrence downstream) would require more process-oriented hazard modeling at a more local scale. A more complex physically based model, typically at the scale of a smaller river catchment, would be required to investigate how the occurrence of one hazard influences the probability of occurrence of another hazard later in time and/or in the same or nearby location (Jenkins et al., 2023). Another significant limitation of this research is the absence of the consideration of stakeholder engagement and feedback while developing and applying the multi-hazard exposure estimation model. Interaction with stakeholders in charge of risk management would help to identify further the challenges posed by exposure to multi-hazard, validate the modeling approach proposed in this research, and specify how the results of such models can best contribute to strengthening the effectiveness of risk management strategies.

## 6 Conclusion

This study produced an integrated approach to assess the climate hazards of floods and wildfires. We explored the assessment of several spatially co-occurring hazards and associated building exposure through an ML modeling approach. Through investigation of the flood and wildfire hazards and the impacts of those hazards on the built environment, our modeling approach consisted of collating a database of recorded hazard footprints, topography, climate, geology, and environment data to input into our model. The approach also consisted of developing ML models for hazard modeling and coding in GEE to produce credible susceptibility and exposure maps. The susceptibility evaluation incorporated a matrix that combined hazards associated with flooding and wildfires. The integration of built-environment data with the multi-hazard map facilitated an assessment of the potential exposure to multi-hazards across the region. Going forward, the potential for digitally generated, multi-hazard, and exposure maps for other climate-related hazards, such as landslides or drought, would further aid the identification of regions susceptible to these disasters and facilitate a rapid assessment of the consequences of these events. This research has demonstrated that effective maps can be developed using readily available and accessible data and ML tools that should help inform communities and regulatory authorities in Vietnam and beyond about the likelihood of risk and impacts from climate-related hazards. This research has the potential to provide clear information that will inform the development and implementation of long-term risk reduction and adaptation strategies. Our findings suggest that ML models such as CART and RF could be used to analyze multi-hazard exposure for various geographical areas particularly susceptible to recurring incidents of wildfires and floods. Our data have shown that these tools can model risk and exposure effectively. However, the applied methods in this study did not

account for the changes in the physical system induced by either floods or wildfires. The multi-hazard exposure maps for the province of Quang Nam offer valuable insights for planners, disaster management specialists, and regional authorities, enabling them to adopt more effective management strategies for minimizing the many hazards present in the area. This approach may also facilitate the development of comprehensive strategies that address areas of high exposure to both hazards rather than focusing on individual hazards.

## Appendix A: Influencing factors

Influencing factors related to floods and wildfires are summarized in Table A1, and thematic maps are presented in Fig. A1.

### (i) Elevation

Low-lying areas act as natural drainage basins and are prone to flood occurrences as streams and rivers flow from higher to lower elevations (Komolafe et al., 2020). High areas can act as natural barriers that slow the spread of fire events (Sibold et al., 2006). In this study, the elevation data were derived from the Shuttle Radar Topographic Mission (SRTM) digital elevation model (DEM) with a 30 m spatial resolution (<https://earthexplorer.usgs.gov/>, last access: 1 September 2024). The altitude of the study area varies from 0 to 2573 m.

### (ii) Slope

Slope is another important terrain characteristic significantly influencing flood and wildfire occurrences (Pourghasemi et al., 2020). Steep slopes and increased flow velocity can lead to riverbank erosion and subsequent flooding downstream (Guo et al., 2022). In addition, flat slopes can lead to concentrated floods where water may stagnate or flow less rapidly (Zaharia et al., 2017). On the other hand, steep slopes can either mitigate or accelerate the spread of wildfires under the impact of wind (Eftekharian et al., 2019). The slope data are calculated from the DEM data.

### (iii) Slope aspect

Slope aspect provides information about the direction of a slope face and may play a significant role in flood and fire formations (Vasilakos et al., 2009). In forestry, south-facing slopes in many areas are often drier and more susceptible to wildfires due to increased sunlight exposure and lower moisture levels (Adab et al., 2013). The aspect data are also calculated from the DEM.

### (iv) Slope curvature

Slope curvature refers to the rate of slope change along the land's surface and contributes actively to flood and wildfire

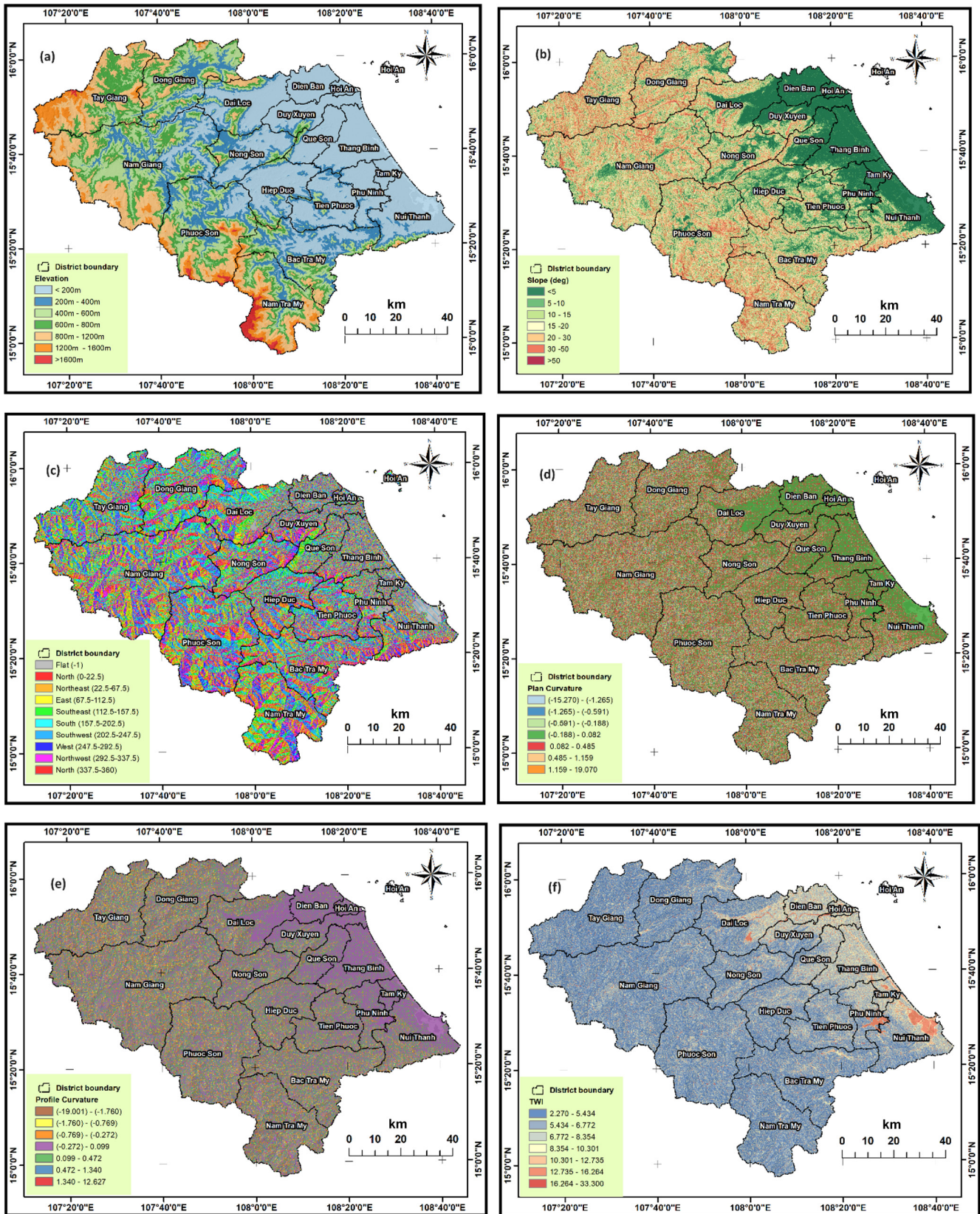


Figure A1.

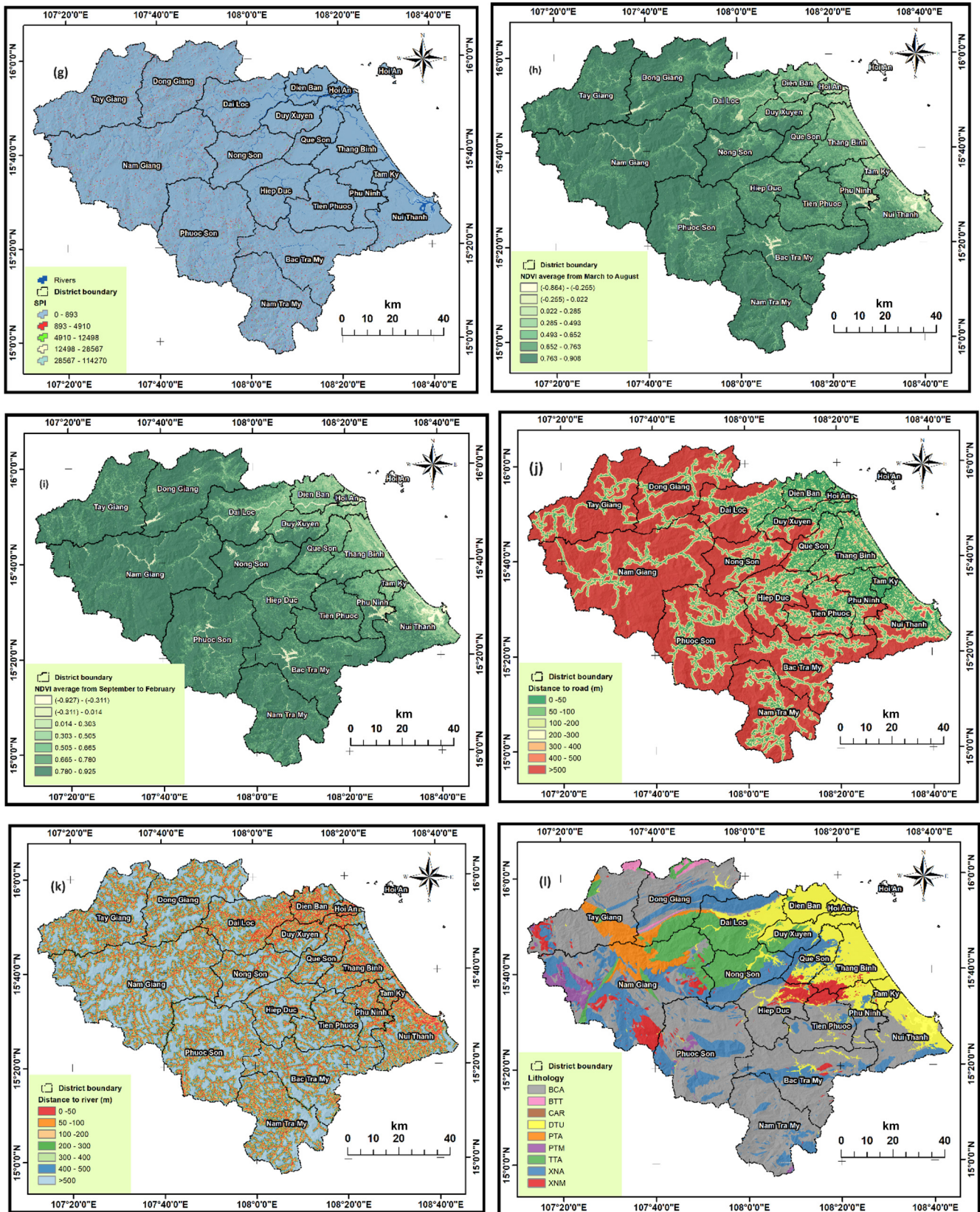
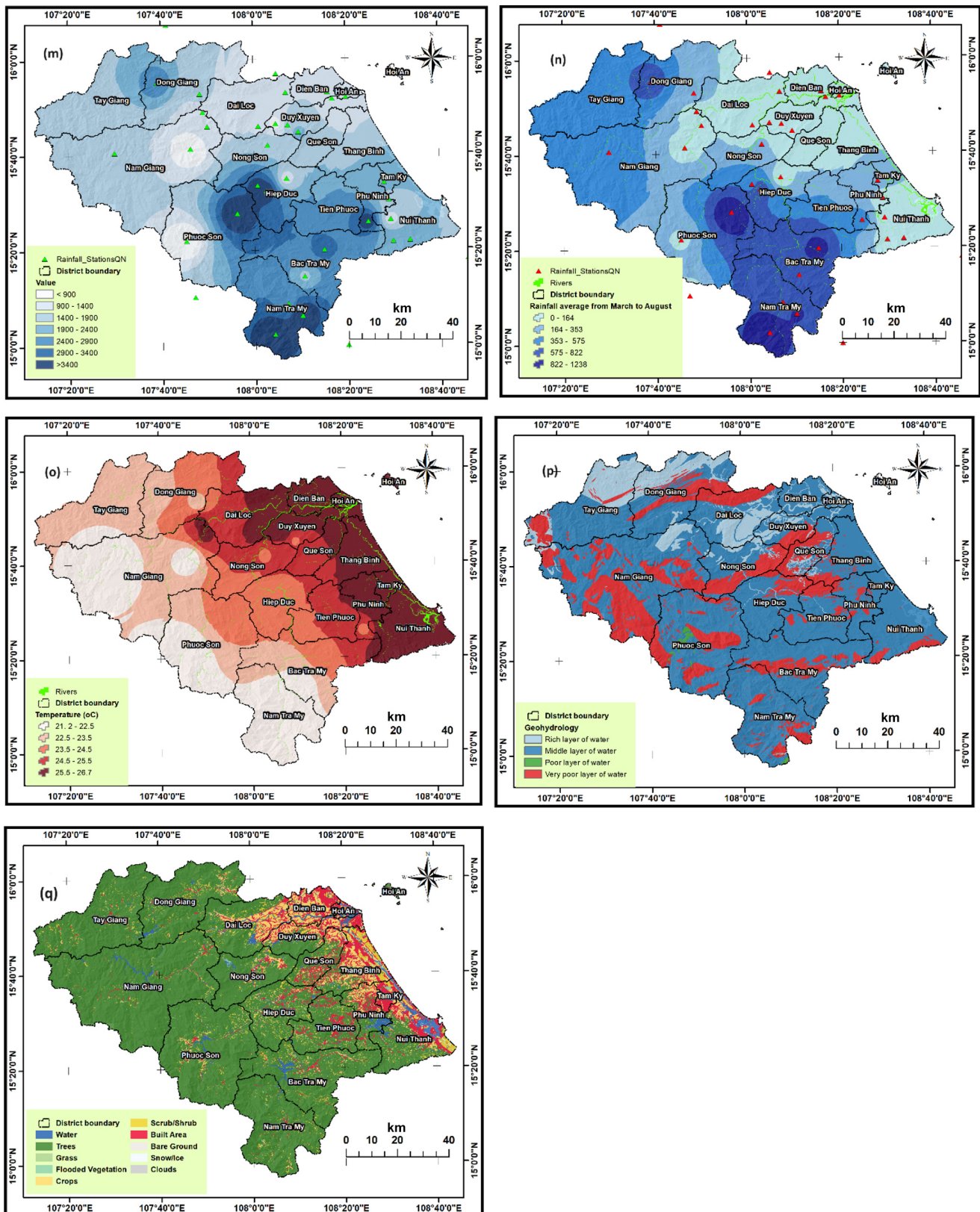


Figure A1.



**Figure A1.** Factors influencing flood and wildfire: (a) elevation, (b) slope, (c) aspect, (d) plan curvature, (e) profile curvature, (f) TWI, (g) SPI, (h) NDVI in dry season, (i) NDVI in rainy season, (j) distance from roads, (k) distance from rivers, (l) lithology, (m) rainfall in rainy season, (n) rainfall in dry season, (o) temperature, (p) geohydrology, and (q) land cover.

**Table A1.** Potential factors affecting flood and forest fire in the province of Quang Nam (where X indicates a potential influencing factor, and 0 indicates no influence).

No.	Used factors	Flood influencing factors	Wildfire influencing factors
1	Elevation	X	X
2	Slope	X	X
3	Aspect	X	X
4	Plan curvature	X	X
5	Profile curvature	X	X
6	TWI	X	0
7	SPI	X	0
8	NDVI		
	– In rainy season	X	0
	– In dry season	0	X
9	Distance from roads	X	X
10	Distance from rivers	X	X
11	Land cover	X	X
12	Average rainfall		
	– In rainy season	X	0
	– In dry season	0	X
13	Average temperature	0	X
14	Lithology	X	X
15	Geohydrology	X	X

formations (Minár et al., 2020). Concave or depressional terrains (negative curvature) can trap water during heavy rainfall, leading to temporary ponding or small-scale flooding in these regions (Mohamed, 2020). Concave curvature can accumulate dead plant material, creating a higher fuel load and increasing the hazard of forest fires (Banerjee, 2021). This study calculates the plan curvature and profile curvature from the DEM.

**(v) TWI and SPI**

The topographic wetness index (TWI) is a topographic parameter used to quantify the propensity of accumulated water in a specific area (Meles et al., 2020). TWI helps identify low-lying areas in the landscape of accumulated water, making it valuable for flood hazard mapping (Nandi et al., 2016). Areas with higher TWI values generally indicate higher accumulated water locations and higher moisture content in the soil and vegetation (Berhanu and Bisrat, 2018). The TWI can be calculated using the following equation (Beven and Kirkby, 1979):

$$TWI = \ln \left( \frac{A_S}{\tan \varepsilon} \right), \tag{A1}$$

where  $\varepsilon$  represents the slope angle in degrees, and  $A_S$  signifies the specific basin area in square meters per meter.

The stream power index (SPI) quantifies the erosive power of flowing water in a stream network. SPI helps assess the potential for erosion and sediment transport within river channels (Zakerinejad and Maerker, 2015). The SPI is identified as follows (Moore et al., 1991):

$$SPI = A_S \times \tan \varepsilon. \tag{A2}$$

This study calculates TWIs and SPIs from the DEM.

**(vi) NDVI**

The normalized difference vegetation index (NDVI) assesses the density of vegetation by calculating the disparity between near-infrared and red-light wavelengths (Bhandari et al., 2012). The sudden decrease in NDVI values could signify changes in current vegetation health due to natural hazards (flood, fire, drought, landslide) or human activities (Teodoro and Duarte, 2022). Areas with high NDVI values may indicate dense vegetation, especially during dry seasons, which can act as significant material for forest fires (Lambert et al., 2015). The NDVI can be calculated as follows:

$$NDVI = \frac{NIR - red}{NIR + red}, \tag{A3}$$

where NIR denotes the near-infrared segment of the electromagnetic spectrum (750–1100 nm), and red corresponds to the red segment of the electromagnetic spectrum (600–750 nm).

This study calculated the spatial distribution of NDVI from the Landsat 8 imagery. The NDVI is the average value for the rainy and dry seasons separately from 2020 to 2023.

**(vii) Distance from roads and distance from rivers**

Distance from roads is a potential controlling factor in flood and wildfire occurrences. They can exacerbate both flood and forest fire events because roads may serve as pathways for water runoff during heavy rainfall and for fire spread in dry conditions (Yousefi et al., 2020). Distance from roads and associated embankments can hamper natural floodplains, causing accumulated water during heavy rains (Douven and Burman, 2013). Moreover, roads with impermeable surfaces can increase surface runoff by preventing water from infiltrating the ground (Yu et al., 2021). Distance from roads can generate potential ignition sources and facilitate firefighting movement (Wang et al., 2015). The 1 : 50 000 study area road network map was created from the 2019 national road network map from the Department of Survey, Mapping, and Geographic Information.

Distance from rivers may influence flood and fire occurrences due to their dynamic relationships with topography, hydrology, and vegetation (Pouyan et al., 2021). Rivers naturally overflow during heavy rainfall, making neighboring areas and floodplains highly susceptible to flooding (Desalegn and Mulu, 2021). Rivers attract human settlements and recreational activities (Gibeau et al., 2002), so areas near rivers are prone to ignition from human-induced sources, especially during dry seasons (Ye et al., 2017). However, distance from rivers also ensures a readily available water supply and makes the ground and vegetation wet due to shallow groundwater, reducing wildfire susceptibility. The study area's river network map on a 1 : 50 000 scale was also collected from the Department of Survey, Mapping, and Geographic Information in 2019.

#### (viii) Land cover

Different land cover types have varying abilities to absorb water, so they may also contribute to the occurrence of floods and wildfires (Agus et al., 2020). Natural land cover features such as floodplains and wetlands act as natural buffers during floods (Fasching et al., 2019). Loss of these areas due to urbanization or deforestation increases the occurrence frequency of flood events (Cirella and Iyalomhe, 2018). Different land cover types, such as dense forests, grasslands, shrublands, and dead vegetation, contribute to accumulating materials for fires (Agus et al., 2020). This study extracted the land cover data from Sentinel-2 optical imagery for 2021 using the deep learning method (<https://livingatlas.arcgis.com/landcover/>, last access: 1 September 2024).

#### (ix) Lithology and geohydrology

Lithology is concerned with bedrock types and their mineralogical properties, significantly influencing soil composition (Gray et al., 2016). The lithological characteristics of an area can indirectly influence wildfire behavior (Pourghasemi et al., 2020). Some rock types, such as shale or coal, can affect the spreading rate of wildfire events (Lu et al., 2021). Lithology also affects the permeability of geological formations and directly contributes to flood occurrences (Jansen, 2006). Impermeable rocks, like crystalline rock or bedrock, can facilitate increased surface runoff during heavy rainfall, resulting in the formation of floods or flash floods (Langston and Temme, 2019). The 1 : 50 000 lithological map of the province of Quang Nam was provided by the Ministry of Natural Resources and Environment of Vietnam for the 2021 data, including nine classes: magma neutral intrusive rocks, aluminosilicate metamorphic rocks, detrital sedimentary rocks, quartz-rich greenstone metamorphic rocks, ultramafic volcanic eruption rocks, carbonate rocks, mafic-ultramafic intrusive rocks, neutral volcanic eruption rocks, and quartz-rich metamorphic and volcanoclastic rocks.

Geohydrology is the study of the movement and availability of groundwater and plays a vital role in influencing vegetation development (Orellana et al., 2012). Geohydrology plays a crucial role in understanding and predicting flood formations based on the presence of aquifers (Lauer et al., 2014). The movement and distribution of groundwater directly impact the behavior of surface water during heavy rainfall (Chen and Hu, 2004). In addition, geohydrology indirectly influences forest fire occurrences because of its impact on soil moisture, land subsidence, and aquifer characteristics (Wösten et al., 2008). Low groundwater levels due to geological formations may lead to dead vegetation, leading to a higher susceptibility to ignition and fire spread (Hasan et al., 2023). The geohydrological map at a 1 : 50 000 scale was provided by the Ministry of Natural Resources and Environment of Vietnam in 2020.

#### (x) Rainfall

In both flood and wildfire occurrences, the amount, intensity, and duration of rainfall may play a role (Stoof et al., 2012). Heavy and prolonged rainfall can lead to increased water flow into rivers and streams and can contribute to the complex dynamics of flood distribution (Khan, 2013). In contrast, insufficient rainfall over an extended period leads to drought conditions, drying out forests and creating ideal conditions for wildfires (Cochrane and Barber, 2009). Daily rainfall data were recorded from 2003 to 2023 and collected from 33 rain gauge stations in the province of Quang Nam. This study used the *inverse distance weighting* technique to separately generate average yearly cumulated rainfall maps for the rainy and dry seasons.

#### (xi) Temperature

The average monthly temperature in the dry months is often closely related to wildfire occurrences (Kumari and Pandey, 2020). In a climate change context, higher average temperatures can increase evaporation and transpiration rates, drying out vegetation that can facilitate fires to ignite and spread rapidly (Houston, 2006). Rising high temperatures can extend the duration of fire events (Sun et al., 2019). The daily temperature data were collected from March to August between 2020 and 2023 (dry seasons) at <https://power.larc.nasa.gov/data-access-viewer/> (last access: 1 September 2024). This research used the inverse distance weighting approach to produce a temperature map for dry seasons (March to August).

*Code availability.* The code will be provided by contacting corresponding author.

*Data availability.* The datasets used in the article are open to the public without restrictions:

- Wildfire locations were accessed via the National Forest Protection Department’s website at <https://watch.pcccr.vn/thongKe/diemChay/>. (National Forest Protection Department, 2024)
- The building dataset was accessed via [https://developers.google.com/earth-engine/datasets/catalog/GOOGLE\\_Research\\_open-buildings\\_v3\\_polygons](https://developers.google.com/earth-engine/datasets/catalog/GOOGLE_Research_open-buildings_v3_polygons) (Earth Engine Data Catalog, 2024).
- Daily temperature data were collected at <https://power.larc.nasa.gov/data-access-viewer/> (NASA, 2024).
- Land cover data from Sentinel-2 optical imagery for 2021 were accessed via <https://livingatlas.arcgis.com/landcover/> (Esri, 2024).
- The digital elevation model (DEM) with a 30 m spatial resolution was extracted from <https://earthexplorer.usgs.gov/> (USGS, 2024).

*Supplement.* The supplement related to this article is available online at: <https://doi.org/10.5194/nhess-24-4385-2024-supplement>.

*Competing interests.* The contact author has declared that none of the authors has any competing interests.

*Disclaimer.* Publisher’s note: Copernicus Publications remains neutral with regard to jurisdictional claims made in the text, published maps, institutional affiliations, or any other geographical representation in this paper. While Copernicus Publications makes every effort to include appropriate place names, the final responsibility lies with the authors.

*Acknowledgements.* We sincerely thank the British Council for funding the UK/Viet Nam Season 2023 project “Evaluation of risks from multi-natural hazards and enhancing community adaptation capacities for Vietnam”. We also acknowledge additional financial support from the VLIRUOS TEAM Project (grant no. VN2022TEA533A105), “GEOdata infrastructures and citizen SCIences to support REsilient development of rural communities in Quang Nam province (GEOSCIRE)”, for the publication of this article.

*Financial support.* This research has been supported by the British Council (grant no. 0037; UK/Viet Nam Season 2023 project “Evaluation of risks from multi-natural hazards and enhancing community adaptation capacities for Vietnam”) and VLIRUOS (grant no. VN2022TEA533A105, TEAM project “GEOdata infrastructures and citizen SCIences to support REsilient development of rural communities in Quang Nam province (GEOSCIRE)”).

*Review statement.* This paper was edited by Robert Sakic Trogrlic and reviewed by Julius Schlumberger, Neiler Medina, and Davide Mauro Ferrario.

## References

- Abedi Gheshlaghi, H., Feizizadeh, B., Blaschke, T., Lakes, T., and Tajbar, S.: Forest fire susceptibility modeling using hybrid approaches, *T. GIS*, 25, 311–333, <https://doi.org/10.1111/tgis.12688>, 2021.
- Abram, N. J., Henley, B. J., Sen Gupta, A., Lippmann, T. J. R., Clarke, H., Dowdy, A. J., Sharples, J. J., Nolan, R. H., Zhang, T., Wooster, M. J., Wurtzel, J. B., Meissner, K. J., Pitman, A. J., Ukkola, A. M., Murphy, B. P., Tapper, N. J., and Boer, M. M.: Connections of climate change and variability to large and extreme forest fires in southeast Australia, *Commun. Earth Environ.*, 2, 8, <https://doi.org/10.1038/s43247-020-00065-8>, 2021.
- Adab, H., Kanniah, K. D., and Solaimani, K.: Modeling forest fire risk in the northeast of Iran using remote sensing and GIS techniques, *Nat. Hazards*, 65, 1723–1743, <https://doi.org/10.1007/s11069-012-0450-8>, 2013.
- Agus, C., Ilfana, Z., Azmi, F., Rachmanadi, D., Widiyatno, Wulandari, D., Santosa, P., Harun, M., Yuwati, T., and Lestari, T.: The effect of tropical peat land-use changes on plant diversity and soil properties, *Int. J. Environ. Sci. Te.*, 17, 1703–1712, <https://doi.org/10.1007/s13762-019-02579-x>, 2020.
- Ahmadlou, M., Karimi, M., Alizadeh, S., Shirzadi, A., Parvinnejhad, D., Shahabi, H., and Panahi, M.: Flood susceptibility assessment using integration of adaptive network-based fuzzy inference system (ANFIS) and biogeography-based optimization (BBO) and BAT algorithms (BA), *Geocarto Int.*, 34, 1252–1272, <https://doi.org/10.1080/10106049.2018.1474276>, 2018.
- Ahmadlou, M., Ebrahimian Ghajari, Y., and Karimi, M.: Enhanced classification and regression tree (CART) by genetic algorithm (GA) and grid search (GS) for flood susceptibility mapping and assessment, *Geocarto Int.*, 37, 13638–13657, <https://doi.org/10.1080/10106049.2022.2082550>, 2022.
- Ansori, S.: The Politics of Forest Fires in Southeast Asia, *Contemp. S. E. Asia*, 43, 179–202, 2021.
- Arabameri, A., Pradhan, B., Rezaei, K., Yamani, M., Pourghasemi, H. R., and Lombardo, L.: Spatial modelling of gully erosion using evidential belief function, logistic regression, and a new ensemble of evidential belief function–logistic regression algorithm, *Land Degrad. Dev.*, 29, 4035–4049, <https://doi.org/10.1002/ldr.3151>, 2018.
- Askar, R., Bragança, L., and Gervásio, H.: Adaptability of Buildings: A Critical Review on the Concept Evolution, *Appl. Sci.*, 11, 4483, <https://doi.org/10.3390/app11104483>, 2021.
- Balica, S. F., Dinh, Q., and Popescu, I.: Chapter 5 – Vulnerability and Exposure in Developed and Developing Countries: Large-Scale Assessments, in: *Hydro-Meteorological Hazards, Risks and Disasters*, edited by: Baldassarre, J. F., Paron, P. and Di Baldassarre, G., Elsevier, Boston, <https://doi.org/10.1016/B978-0-12-394846-5.00005-9>, 125–162, 2015.
- Banerjee, P.: Maximum entropy-based forest fire likelihood mapping: analysing the trends, distribution, and drivers of forest fires in Sikkim Himalaya, *Scand. J. Forest Res.*, 36, 275–288, <https://doi.org/10.1080/02827581.2021.1918239>, 2021.

- Bangalore, M., Smith, A., and Veldkamp, T.: Exposure to Floods, Climate Change, and Poverty in Vietnam, *Economics of Disasters and Climate Change*, 3, 79–99, <https://doi.org/10.1007/s41885-018-0035-4>, 2018.
- Berhanu, B. and Bisrat, E.: Identification of surface water storing sites using topographic wetness index (TWI) and normalized difference vegetation index (NDVI), *Journal of Natural Resources and Development*, 8, 91–100, <https://doi.org/10.5027/jnrd.v8i0.09>, 2018.
- Beven, K. J. and Kirkby, M. J.: A physically based, variable contributing area model of basin hydrology/Un modèle à base physique de zone d'appel variable de l'hydrologie du bassin versant, *Hydrolog. Sci. B.*, 24, 43–69, <https://doi.org/10.1080/02626667909491834>, 1979.
- Bhandari, A. K., Kumar, A., and Singh, G. K.: Feature Extraction using Normalized Difference Vegetation Index (NDVI): A Case Study of Jabalpur City, *Proc. Tech.*, 6, 612–621, <https://doi.org/10.1016/j.procty.2012.10.074>, 2012.
- Bountzouklis, C., Fox, D. M., and Di Bernardino, E.: Environmental factors affecting wildfire-burned areas in southeastern France, 1970–2019, *Nat. Hazards Earth Syst. Sci.*, 22, 1181–1200, <https://doi.org/10.5194/nhess-22-1181-2022>, 2022.
- Breiman, L.: Random Forests, *Mach. Learn.*, 45, 5–32, <https://doi.org/10.1023/a:1010933404324>, 2001.
- Breiman, L., Friedman, J., Olshen, R. A., and Stone, C. J.: Classification and Regression Trees, in: 1st Edn., Chapman and Hall/CRC, <https://doi.org/10.1201/9781315139470>, 1984.
- Bui, Q. D., Luu, C., Mai, S. H., Ha, H. T., Ta, H. T., and Pham, B. T.: Flood risk mapping and analysis using an integrated framework of machine learning models and analytic hierarchy process, *Risk Anal.*, 43, 1478–1495, <https://doi.org/10.1111/risa.14018>, 2023a.
- Bui, Q. D., Ha, H., Khuc, D. T., Nguyen, D. Q., von Meding, J., Nguyen, L. P., and Luu, C.: Landslide susceptibility prediction mapping with advanced ensemble models: Son La province, Vietnam, *Nat. Hazards*, 116, 2283–2309, <https://doi.org/10.1007/s11069-022-05764-3>, 2023b.
- Carreño, M. L., Cardona, O. D., and Barbat, A. H.: A disaster risk management performance index, *Nat. Hazards*, 41, 1–20, <https://doi.org/10.1007/s11069-006-9008-y>, 2007.
- Carter, J. V., Pan, J., Rai, S. N., and Galandiuk, S.: ROC-ing along: Evaluation and interpretation of receiver operating characteristic curves, *Surgery*, 159, 1638–1645, <https://doi.org/10.1016/j.surg.2015.12.029>, 2016.
- Chau, V. N., Cassells, S., and Holland, J.: Economic impact upon agricultural production from extreme flood events in Quang Nam, central Vietnam, *Nat. Hazards*, 75, 1747–1765, <https://doi.org/10.1007/s11069-014-1395-x>, 2014.
- Chen, W., Xie, X., Peng, J., Shahabi, H., Hong, H., Bui, D. T., Duan, Z., Li, S., and Zhu, A. X.: GIS-based landslide susceptibility evaluation using a novel hybrid integration approach of bivariate statistical based random forest method, *CATENA*, 164, 135–149, <https://doi.org/10.1016/j.catena.2018.01.012>, 2018.
- Chen, X. and Hu, Q.: Groundwater influences on soil moisture and surface evaporation, *J. Hydrol.*, 297, 285–300, <https://doi.org/10.1016/j.jhydrol.2004.04.019>, 2004.
- Cirella, G. T. and Iyalomhe, F. O.: Flooding conceptual review: Sustainability-focused best practices in Nigeria, *Appl. Sci.*, 8, 1558, <https://doi.org/10.3390/app8091558>, 2018.
- Cochrane, M. A. and Barber, C. P.: Climate change, human land use and future fires in the Amazon, *Glob. Change Biol.*, 15, 601–612, <https://doi.org/10.1111/j.1365-2486.2008.01786.x>, 2009.
- De Angeli, S., Malamud, B. D., Rossi, L., Taylor, F. E., Trasforini, E., and Rudari, R.: A multi-hazard framework for spatial-temporal impact analysis, *Int. J. Disast. Risk Re.*, 73, 102829, <https://doi.org/10.1016/j.ijdr.2022.102829>, 2022.
- Desalegn, H. and Mulu, A.: Mapping flood inundation areas using GIS and HEC-RAS model at Fetam River, Upper Abbay Basin, Ethiopia, *Scientific African*, 12, e00834, <https://doi.org/10.1016/j.sciaf.2021.e00834>, 2021.
- Dottori, F., Martina, M. L. V., and Figueiredo, R.: A methodology for flood susceptibility and vulnerability analysis in complex flood scenarios, *J. Flood Risk Manag.*, 11, S632–S645, <https://doi.org/10.1111/jfr3.12234>, 2018.
- Douven, W. and Buurman, J.: Planning practice in support of economically and environmentally sustainable roads in floodplains: The case of the Mekong delta floodplains, *J. Environ. Manage.*, 128, 161–168, <https://doi.org/10.1016/j.jenvman.2013.04.048>, 2013.
- Du, T. L. T., Bui, D. D., Nguyen, M. D., and Lee, H.: Satellite-Based, Multi-Indices for Evaluation of Agricultural Droughts in a Highly Dynamic Tropical Catchment, Central Vietnam, *Water*, 10, 659, <https://doi.org/10.3390/w10050659>, 2018.
- Earth Engine Data Catalog: Open Buildings V3 Polygons, Earth Engine Data Catalog [data set], [https://developers.google.com/earth-engine/datasets/catalog/GOOGLE\\_Research\\_open-buildings\\_v3\\_polygons](https://developers.google.com/earth-engine/datasets/catalog/GOOGLE_Research_open-buildings_v3_polygons) (last access: 3 December 2024), 2024.
- Eftekharian, E., Ghodrat, M., He, Y., Ong, R. H., Kwok, K. C. S., Zhao, M., and Samali, B.: Investigation of terrain slope effects on wind enhancement by a line source fire, *Case Studies in Thermal Engineering*, 14, 100467, <https://doi.org/10.1016/j.csite.2019.100467>, 2019.
- Eisenbies, M. H., Aust, W. M., Burger, J. A., and Adams, M. B.: Forest operations, extreme flooding events, and considerations for hydrologic modeling in the Appalachians—A review, *Forest Ecol. Manag.*, 242, 77–98, <https://doi.org/10.1016/j.foreco.2007.01.051>, 2007.
- Esri: Sentinel-2 10-Meter Land Use/Land Cover, Esri [data set], <https://livingatlas.arcgis.com/landcover/> (last access: 3 December 2024), 2024.
- Fasching, C., Wilson, H. F., D'Amario, S. C., and Xenopoulos, M. A.: Natural land cover in agricultural catchments alters flood effects on DOM composition and decreases nutrient levels in streams, *Ecosystems*, 22, 1530–1545, <https://doi.org/10.1007/s10021-019-00354-0>, 2019.
- Fox, E. W., Hill, R. A., Leibowitz, S. G., Olsen, A. R., Thornbrugh, D. J., and Weber, M. H.: Assessing the accuracy and stability of variable selection methods for random forest modeling in ecology, *Environ. Monit. Assess.*, 189, 1–20, <https://doi.org/10.1007/s10661-017-6025-0>, 2017.
- Gan, C. C. R., Oktari, R. S., Nguyen, H. X., Yuan, L., Yu, X., Kc, A., Hanh, T. T. T., Phung, D. T., Dwirahmadi, F., Liu, T., Musumari, P. M., Kayano, R., and Chu, C.: A scoping review of climate-related disasters in China, Indonesia and Vietnam: Disasters, health impacts, vulnerable populations and adaptation measures, *Int. J. Disast. Risk Re.*, 66, 102608, <https://doi.org/10.1016/j.ijdr.2021.102608>, 2021.

- Genuer, R., Poggi, J.-M., and Tuleau-Malot, C.: Variable selection using random forests, *Pattern Recogn. Lett.*, 31, 2225–2236, <https://doi.org/10.1016/j.patrec.2010.03.014>, 2010.
- Gibeau, M. L., Clevenger, A. P., Herrero, S., and Wierzychowski, J.: Grizzly bear response to human development and activities in the Bow River Watershed, Alberta, Canada, *Biol. Conserv.*, 103, 227–236, [https://doi.org/10.1016/S0006-3207\(01\)00131-8](https://doi.org/10.1016/S0006-3207(01)00131-8), 2002.
- Giglio, L., Csiszar, I., Restás, Á., Morissette, J. T., Schroeder, W., Morton, D., and Justice, C. O.: Active fire detection and characterization with the advanced spaceborne thermal emission and reflection radiometer (ASTER), *Remote Sens. Environ.*, 112, 3055–3063, <https://doi.org/10.1016/j.rse.2008.03.003>, 2008.
- Gonzalez-Arqueros, M. L., Mendoza, M. E., Bocco, G., and Solis Castillo, B.: Flood susceptibility in rural settlements in remote zones: The case of a mountainous basin in the Sierra-Costa region of Michoacan, Mexico, *J. Environ. Manage.*, 223, 685–693, <https://doi.org/10.1016/j.jenvman.2018.06.075>, 2018.
- Gray, J. M., Bishop, T. F. A., and Wilford, J. R.: Lithology and soil relationships for soil modelling and mapping, *CATENA*, 147, 429–440, <https://doi.org/10.1016/j.catena.2016.07.045>, 2016.
- Guo, X., Ge, Y., Zhan, M., and Yan, H.: Failure process of a lateral slope deposit and its effect on debris flood formation, *B. Eng. Geol. Environ.*, 81, 324, <https://doi.org/10.1007/s10064-022-02789-7>, 2022.
- Ha, H., Bui, Q. D., Khuc, T. D., Tran, D. T., Pham, B. T., Mai, S. H., Nguyen, L. P., and Luu, C.: A machine learning approach in spatial predicting of landslides and flash flood susceptible zones for a road network, *Model. Earth Syst. Environ.*, 8, 4341–4357, <https://doi.org/10.1007/s40808-022-01384-9>, 2022.
- Ha, H., Bui, Q. D., Nguyen, H. D., Pham, B. T., Lai, T. D., and Luu, C.: A practical approach to flood hazard, vulnerability, and risk assessing and mapping for Quang Binh province, Vietnam, *Environ. Dev. Sustain.*, 25, 1101–1130, <https://doi.org/10.1007/s10668-021-02041-4>, 2023.
- Hasan, M. F., Smith, R., Vajedian, S., Pommerenke, R., and Majumdar, S.: Global land subsidence mapping reveals widespread loss of aquifer storage capacity, *Nat. Commun.*, 14, 6180, <https://doi.org/10.1038/s41467-023-41933-z>, 2023.
- Hasanzadeh Nafari, R., Ngo, T., and Mendis, P.: An Assessment of the Effectiveness of Tree-Based Models for Multi-Variate Flood Damage Assessment in Australia, *Water*, 8, 282, <https://doi.org/10.3390/w8070282>, 2016.
- Hosseini, M. and Lim, S.: Gene expression programming and data mining methods for bushfire susceptibility mapping in New South Wales, Australia, *Nat. Hazards*, 113, 1349–1365, <https://doi.org/10.1007/s11069-022-05350-7>, 2022.
- Houston, J.: Evaporation in the Atacama Desert: An empirical study of spatio-temporal variations and their causes, *J. Hydrol.*, 330, 402–412, <https://doi.org/10.1016/j.jhydrol.2006.03.036>, 2006.
- IPCC: Climate Change 2022: Impacts, Adaptation and Vulnerability, Working Group II Contribution to the Sixth Assessment Report of the Intergovernmental Panel on Climate Change, Cambridge University Press, <https://doi.org/10.1017/9781009325844.002>, 2022.
- Jansen, J. D.: Flood magnitude–frequency and lithologic control on bedrock river incision in post-orogenic terrain, *Geomorphology*, 82, 39–57, <https://doi.org/10.1016/j.geomorph.2005.08.018>, 2006.
- Javidan, N., Kavian, A., Pourghasemi, H. R., Conoscenti, C., Jafarian, Z., and Rodrigo-Comino, J.: Evaluation of multi-hazard map produced using MaxEnt machine learning technique, *Sci. Rep.*, 11, 6496, <https://doi.org/10.1038/s41598-021-85862-7>, 2021.
- Jenkins, L. T., Creed, M. J., Tarbali, K., Muthusamy, M., Trogrlić, R. Š., Phillips, J. C., Watson, C. S., Sinclair, H. D., Galasso, C., and McCloskey, J.: Physics-based simulations of multiple natural hazards for risk-sensitive planning and decision making in expanding urban regions, *Int. J. Disast. Risk Re.*, 84, <https://doi.org/10.1016/j.ijdr.2022.103338>, 2023.
- Kalantar, B., Ueda, N., Idrees, M. O., Janizadeh, S., Ahmadi, K., and Shabani, F.: Forest fire susceptibility prediction based on machine learning models with resampling algorithms on remote sensing data, *Remote Sens.-Basel*, 12, 3682, <https://doi.org/10.3390/rs12223682>, 2020.
- Khan, A., Gupta, S., and Gupta, S. K.: Multi-hazard disaster studies: Monitoring, detection, recovery, and management, based on emerging technologies and optimal techniques, *Int. J. Disast. Risk Re.*, 47, 101642, <https://doi.org/10.1016/j.ijdr.2020.101642>, 2020.
- Khan, A. N.: Analysis of 2010-flood causes, nature and magnitude in the Khyber Pakhtunkhwa, Pakistan, *Nat. Hazards*, 66, 887–904, <https://doi.org/10.1007/s11069-012-0528-3>, 2013.
- Khatakho, R., Gautam, D., Aryal, K. R., Pandey, V. P., Rupakhety, R., Lamichhane, S., Liu, Y.-C., Abdouli, K., Talchabadel, R., and Thapa, B. R.: Multi-hazard risk assessment of Kathmandu Valley, Nepal, *Sustainability*, 13, 5369, <https://doi.org/10.3390/su13105369>, 2021.
- Kim, J.-C., Lee, S., Jung, H.-S., and Lee, S.: Landslide susceptibility mapping using random forest and boosted tree models in Pyeong-Chang, Korea, *Geocarto Int.*, 33, 1000–1015, <https://doi.org/10.1080/10106049.2017.1323964>, 2017.
- Komolafe, A., Awe, B., Olorunfemi, I., and Oguntunde, P.: Modelling flood-prone area and vulnerability using integration of multi-criteria analysis and HAND model in the Ogun River Basin, Nigeria, *Hydrolog. Sci. J.*, 65, 1766–1783, <https://doi.org/10.1080/02626667.2020.1764960>, 2020.
- Kumari, B. and Pandey, A. C.: MODIS based forest fire hotspot analysis and its relationship with climatic variables, *Spatial Information Research*, 28, 87–99, <https://doi.org/10.1007/s41324-019-00275-z>, 2020.
- Lambert, J., Denux, J.-P., Verbesselt, J., Balent, G., and Cheret, V.: Detecting clear-cuts and decreases in forest vitality using MODIS NDVI time series, *Remote Sens.-Basel*, 7, 3588–3612, <https://doi.org/10.3390/rs70403588>, 2015.
- Langston, A. L. and Temme, A. J. A. M.: Bedrock erosion and changes in bed sediment lithology in response to an extreme flood event: The 2013 Colorado Front Range flood, *Geomorphology*, 328, 1–14, <https://doi.org/10.1016/j.geomorph.2018.11.015>, 2019.
- Lauber, U., Kotyla, P., Morche, D., and Goldscheider, N.: Hydrogeology of an Alpine rockfall aquifer system and its role in flood attenuation and maintaining baseflow, *Hydrol. Earth Syst. Sci.*, 18, 4437–4452, <https://doi.org/10.5194/hess-18-4437-2014>, 2014.
- Lee, J., Perera, D., Glickman, T., and Taing, L.: Water-related disasters and their health impacts: A global review, *Progress in Disaster Science*, 8, 100123, <https://doi.org/10.1016/j.pdisas.2020.100123>, 2020.

- Lu, M., Ikejiri, T., and Lu, Y.: A synthesis of the Devonian wildfire record: Implications for paleogeography, fossil flora, and paleoclimate, *Palaeogeogr. Palaeoclimatol.*, 571, 110321, <https://doi.org/10.1016/j.palaeo.2021.110321>, 2021.
- Luu, C., Von Meding, J., and Kanjanabootra, S.: Assessing flood hazard using flood marks and analytic hierarchy process approach: a case study for the 2013 flood event in Quang Nam, Vietnam, *Nat. Hazards*, 90, 1031–1050, <https://doi.org/10.1007/s11069-017-3083-0>, 2018.
- Luu, C., Bui, Q. D., and von Meding, J.: Mapping direct flood impacts from a 2020 extreme flood event in Central Vietnam using spatial analysis techniques, *International Journal of Disaster Resilience in the Built Environment*, 14, 85–99, <https://doi.org/10.1108/ijdrbe-07-2021-0070>, 2021.
- Ma, Y., Ma, B., Jiao, H., Zhang, Y., Xin, J., and Yu, Z.: An analysis of the effects of weather and air pollution on tropospheric ozone using a generalized additive model in Western China: Lanzhou, Gansu, *Atmos. Environ.*, 224, 117342, <https://doi.org/10.1016/j.atmosenv.2020.117342>, 2020.
- Meghanadh, D., Kumar Maurya, V., Tiwari, A., and Dwivedi, R.: A multi-criteria landslide susceptibility mapping using deep multi-layer perceptron network: A case study of Srinagar-Rudraprayag region (India), *Adv. Space Res.*, 2022, 69, 1883–1893, <https://doi.org/10.1016/j.asr.2021.10.021>, 2022.
- Mai Sy, H., Luu, C., Bui, Q. D., Ha, H., and Nguyen, D. Q.: Urban flood risk assessment using Sentinel-1 on the google earth engine: A case study in Thai Nguyen city, Vietnam, *Remote Sensing Applications: Society and Environment*, 31, 100987, <https://doi.org/10.1016/j.rsase.2023.100987>, 2023.
- Meles, M. B., Younger, S. E., Jackson, C. R., Du, E., and Drover, D.: Wetness index based on landscape position and topography (WILT): Modifying TWI to reflect landscape position, *J. Environ. Manage.*, 255, 109863, <https://doi.org/10.1016/j.jenvman.2019.109863>, 2020.
- Menoni, S., Molinari, D., Parker, D., Ballio, F., and Tapsell, S.: Assessing multifaceted vulnerability and resilience in order to design risk-mitigation strategies, *Nat. Hazards*, 64, 2057–2082, <https://doi.org/10.1007/s11069-012-0134-4>, 2012.
- Miao, F., Zhao, F., Wu, Y., Li, L., and Török, Á.: Landslide susceptibility mapping in Three Gorges Reservoir area based on GIS and boosting decision tree model, *Stoch. Env. Res. Risk A.*, 37, 2283–2303, <https://doi.org/10.1007/s00477-023-02394-4>, 2023.
- Minár, J., Evans, I. S., and Jenčo, M.: A comprehensive system of definitions of land surface (topographic) curvatures, with implications for their application in geoscience modelling and prediction, *Earth-Sci. Rev.*, 211, 103414, <https://doi.org/10.1016/j.earscirev.2020.103414>, 2020.
- Mohamed, M. A.: Classification of landforms for digital soil mapping in urban areas using LiDAR data derived terrain attributes: a case study from Berlin, Germany, *Land*, 9, 319, <https://doi.org/10.3390/land9090319>, 2020.
- Moore, I. D., Grayson, R., and Ladson, A.: Digital terrain modelling: a review of hydrological, geomorphological, and biological applications, *Hydrol. Process.*, 5, 3–30, <https://doi.org/10.1002/hyp.3360050103>, 1991.
- Mueller, J. M., Lima, R. E., Springer, A. E., and Schiefer, E.: Using matching methods to estimate impacts of wildfire and postwildfire flooding on house prices, *Water Resour. Res.*, 54, 6189–6201, <https://doi.org/10.1029/2017WR022195>, 2018.
- Nachappa, T., Ghorbanzadeh, O., Gholamnia, K., and Blaschke, T.: Multi-Hazard Exposure Mapping Using Machine Learning for the State of Salzburg, Austria, *Remote Sens.-Basel*, 12, 2757, <https://doi.org/10.3390/rs12172757>, 2020.
- Naghibi, S. A., Pourghasemi, H. R., and Dixon, B.: GIS-based groundwater potential mapping using boosted regression tree, classification and regression tree, and random forest machine learning models in Iran, *Environ. Monit. Assess.*, 188, 1–27, <https://doi.org/10.1007/s10661-015-5049-6>, 2016.
- Nandi, A., Mandal, A., Wilson, M., and Smith, D.: Flood hazard mapping in Jamaica using principal component analysis and logistic regression, *Environ. Earth Sci.*, 75, 1–16, <https://doi.org/10.1007/s12665-016-5323-0>, 2016.
- NASA: The NASA POWER Project's Data Access Viewer, NASA [data set], <https://power.larc.nasa.gov/data-access-viewer/> (last access: 3 December 2024), 2024.
- National Forest Protection Department: <https://watch.pcccr.vn/thongKe/diemChay/> (last access: 5 December 2024), 2024.
- Nguyen, T. V., Allen, K. J., Le, N. C., Truong, C. Q., Tenzin, K., and Baker, P. J.: Human-Driven Fire Regime Change in the Seasonal Tropical Forests of Central Vietnam, *Geophys. Res. Lett.*, 50, e2022GL100687, <https://doi.org/10.1029/2022gl100687>, 2023.
- Orellana, F., Verma, P., Loheide, S. P., and Daly, E.: Monitoring and modeling water-vegetation interactions in groundwater-dependent ecosystems, *Rev. Geophys.*, 50, RG3003, <https://doi.org/10.1029/2011RG000383>, 2012.
- Papaioannou, G., Alamanos, A., and Maris, F.: Evaluating Post-Fire Erosion and Flood Protection Techniques: A Narrative Review of Applications, *GeoHazards*, 4, 380–405, <https://doi.org/10.3390/geoHazards4040022>, 2023.
- Piao, Y., Lee, D., Park, S., Kim, H. G., and Jin, Y.: Multi-hazard mapping of droughts and forest fires using a multi-layer hazards approach with machine learning algorithms, *Geomat. Nat. Haz. Risk*, 13, 2649–2673, <https://doi.org/10.1080/19475705.2022.2128440>, 2022.
- Pourghasemi, H. R., Kariminejad, N., Amiri, M., Edalat, M., Zarafshar, M., Blaschke, T., and Cerda, A.: Assessing and mapping multi-hazard risk susceptibility using a machine learning technique, *Sci. Rep.*, 10, 3203, <https://doi.org/10.1038/s41598-020-60191-3>, 2020.
- Pourghasemi, H. R., Pouyan, S., Bordbar, M., Golkar, F., and Clague, J. J.: Flood, landslides, forest fire, and earthquake susceptibility maps using machine learning techniques and their combination, *Nat. Hazards*, 116, 3797–3816, <https://doi.org/10.1007/s11069-023-05836-y>, 2023.
- Pourtaghi, Z. S., Pourghasemi, H. R., Aretano, R., and Semeraro, T.: Investigation of general indicators influencing on forest fire and its susceptibility modeling using different data mining techniques, *Ecol. Indic.*, 64, 72–84, <https://doi.org/10.1016/j.ecolind.2015.12.030>, 2016.
- Pouyan, S., Pourghasemi, H. R., Bordbar, M., Rahmadian, S., and Clague, J. J.: A multi-hazard map-based flooding, gully erosion, forest fires, and earthquakes in Iran, *Sci. Rep.*, 11, 14889, <https://doi.org/10.1038/s41598-021-94266-6>, 2021.
- Rentschler, J., Salhab, M., and Jafino, B. A.: Flood exposure and poverty in 188 countries, *Nat. Commun.*, 13, 3527, <https://doi.org/10.1038/s41467-022-30727-4>, 2022.
- Rusk, J., Maharjan, A., Tiwari, P., Chen, T.-H. K., Shneiderman, S., Turin, M., and Seto, K. C.: Multi-hazard

- susceptibility and exposure assessment of the Hindu Kush Himalaya, *Sci. Total Environ.*, 804, 150039, <https://doi.org/10.1016/j.scitotenv.2021.150039>, 2022.
- Šakić Trogrlić, R., Thompson, H. E., Menteşe, E. Y., Hus-sain, E., Gill, J. C., Taylor, F. E., Mwangi, E., Öner, E., Bukachi, V. G., and Malamud, B. D.: Multi-Hazard Inter-relationships and Risk Scenarios in Urban Areas: A Case of Nairobi and Istanbul, *Earths Future*, 12, e2023EF004413, <https://doi.org/10.1029/2023ef004413>, 2024.
- Schneiderbauer, S. and Ehrlich, D.: Risk, hazard and people's vulnerability to natural hazards, A review of definitions, concepts and data, *EUR*, 21410, 40, European Commission Joint Research Centre, 2004.
- Schratz, P., Muenchow, J., Iturritxa, E., Richter, J., and Brenning, A.: Hyperparameter tuning and performance assessment of statistical and machine-learning algorithms using spatial data, *Ecol. Model.*, 406, 109–120, <https://doi.org/10.1016/j.ecolmodel.2019.06.002>, 2019.
- Sibold, J. S., Veblen, T. T., and González, M. E.: Spatial and temporal variation in historic fire regimes in subalpine forests across the Colorado Front Range in Rocky Mountain National Park, Colorado, USA, *J. Biogeogr.*, 33, 631–647, <https://doi.org/10.1111/j.1365-2699.2005.01404.x>, 2006.
- Sirko, W., Kashubin, S., Ritter, M., Annkah, A., Bouchareb, Y. S. E., Dauphin, Y., Keyzers, D., Neumann, M., Cisse, M., and Quinn, J.: Continental-scale building detection from high resolution satellite imagery, *arXiv [preprint]*, arXiv:2107.12283, 2021.
- Skilodimou, H. D., Bathrellos, G. D., Chousianitis, K., Youssef, A. M., and Pradhan, B.: Multi-hazard assessment modeling via multi-criteria analysis and GIS: a case study, *Environ. Earth Sci.*, 78, 1–21, <https://doi.org/10.1007/s12665-018-8003-4>, 2019.
- Skilodimou, H. D., Bathrellos, G. D., and Alexakis, D. E.: Flood hazard assessment mapping in burned and urban areas, *Sustainability*, 13, 4455, <https://doi.org/10.3390/su13084455>, 2021.
- Stoof, C. R., Vervoort, R. W., Iwema, J., van den Elsen, E., Ferreira, A. J. D., and Ritsema, C. J.: Hydrological response of a small catchment burned by experimental fire, *Hydrol. Earth Syst. Sci.*, 16, 267–285, <https://doi.org/10.5194/hess-16-267-2012>, 2012.
- Sun, Q., Miao, C., Hanel, M., Borthwick, A. G. L., Duan, Q., Ji, D., and Li, H.: Global heat stress on health, wildfires, and agricultural crops under different levels of climate warming, *Environ. Int.*, 128, 125–136, <https://doi.org/10.1016/j.envint.2019.04.025>, 2019.
- Tamiminia, H., Salehi, B., Mahdianpari, M., Quackenbush, L., Adeli, S., and Brisco, B.: Google Earth Engine for geo-big data applications: A meta-analysis and systematic review, *ISPRS J. Photogramm.*, 164, 152–170, <https://doi.org/10.1016/j.isprsjprs.2020.04.001>, 2020.
- Tang, R. and Zhang, X.: CART decision tree combined with Boruta feature selection for medical data classification, in: 2020 5th IEEE International Conference on Big Data Analytics (ICBDA), 8–11 May 2020, Xiamen, China, 80–84, <https://doi.org/10.1109/ICBDA49040.2020.9101199>, 2020.
- Tavakkoli Pirailou, S., Einali, G., Ghorbanzadeh, O., Nachappa, T. G., Gholamnia, K., Blaschke, T., and Ghamisi, P.: A Google Earth Engine approach for wildfire susceptibility prediction fusion with remote sensing data of different spatial resolutions, *Remote Sens.-Basel*, 14, 672, <https://doi.org/10.3390/rs14030672>, 2022.
- Tedim, F., Xanthopoulos, G., and Leone, V.: Chapter 5 – Forest Fires in Europe: Facts and Challenges, in: *Wildfire Hazards, Risks and Disasters*, edited by: Shroder, J. F., and Patton, D., Elsevier, Oxford, <https://doi.org/10.1016/B978-0-12-410434-1.00005-1>, 77–99, 2015.
- Teodoro, A. C. and Duarte, L.: Chapter 10 – The role of satellite remote sensing in natural disaster management, in: *Nanotechnology-Based Smart Remote Sensing Networks for Disaster Prevention*, edited by: Denizli, A., Alencar, M. S., Nguyen, T. A., and Motaung, D. E., Elsevier, 189–216, <https://doi.org/10.1016/B978-0-323-91166-5.00015-X>, 2022.
- Trang, P. T., Andrew, M. E., Chu, T., and Enright, N. J.: Forest fire and its key drivers in the tropical forests of northern Vietnam, *Int. J. Wildland Fire*, 31, 213–229, <https://doi.org/10.1071/wf21078>, 2022.
- USGS: The U.S. Geological Survey – EarthExplorer, USGS [data set], <https://earthexplorer.usgs.gov/> (last access: 3 December 2024), 2024.
- Vasilakos, C., Kalabokidis, K., Hatzopoulos, J., and Matsinos, I.: Identifying wildland fire ignition factors through sensitivity analysis of a neural network, *Nat. Hazards*, 50, 125–143, <https://doi.org/10.1007/s11069-008-9326-3>, 2009.
- VDMA – Vietnam Disaster Management Authority: Flash Update No. 4: Viet Nam Floods, Landslides and Storms (As of 28 October 2020), <https://phongchongthientai.mard.gov.vn/en/Pages/flash-update-no-4-viet-nam-floods-landslides-and-storms-as-of> (last access: 28 October 2020), 2020.
- Velev, D. and Zlateva, P.: Challenges of artificial intelligence application for disaster risk management, *Int. Arch. Photogramm. Remote Sens. Spatial Inf. Sci.*, XLVIII-M-1-2023, 387–394, <https://doi.org/10.5194/isprs-archives-XLVIII-M-1-2023-387-2023>, 2023.
- Wang, J., He, Z., and Weng, W.: A review of the research into the relations between hazards in multi-hazard risk analysis, *Nat. Hazards*, 104, 2003–2026, <https://doi.org/10.1007/s11069-020-04259-3>, 2020.
- Wang, S.-H., Wang, W.-C., Wang, K.-C., and Shih, S.-Y.: Applying building information modeling to support fire safety management, *Automat. Constr.*, 59, 158–167, <https://doi.org/10.1016/j.autcon.2015.02.001>, 2015.
- Wing, O. E. J., Bates, P. D., Smith, A. M., Sampson, C. C., Johnson, K. A., Fargione, J., and Morefield, P.: Estimates of present and future flood risk in the conterminous United States, *Environ. Res. Lett.*, 13, 034023, <https://doi.org/10.1088/1748-9326/aaac65>, 2018.
- Wösten, J. H. M., Clymans, E., Page, S. E., Rieley, J. O., and Limin, S. H.: Peat–water interrelationships in a tropical peatland ecosystem in Southeast Asia, *CATENA*, 73, 212–224, <https://doi.org/10.1016/j.catena.2007.07.010>, 2008.
- Wu, W., Zhang, Q., Singh, V. P., Wang, G., Zhao, J., Shen, Z., and Sun, S.: A Data-Driven Model on Google Earth Engine for Landslide Susceptibility Assessment in the Hengduan Mountains, the Qinghai–Tibetan Plateau, *Remote Sens.-Basel*, 14, 4662, <https://doi.org/10.3390/rs14184662>, 2022.
- Ye, J., Wu, M., Deng, Z., Xu, S., Zhou, R., and Clarke, K. C.: Modeling the spatial patterns of human wildfire ignition in Yunnan province, China, *Appl. Geogr.*, 89, 150–162, <https://doi.org/10.1016/j.apgeog.2017.09.012>, 2017.

- Yousefi, S., Pourghasemi, H. R., Emami, S. N., Pouyan, S., Eskandari, S., and Tiefenbacher, J. P.: A machine learning framework for multi-hazards modeling and mapping in a mountainous area, *Sci. Rep.*, 10, 12144, <https://doi.org/10.1038/s41598-020-69233-2>, 2020.
- Yu, G., Liu, T., McGuire, L. A., Wright, D. B., Hatchett, B. J., Miller, J. J., Berli, M., Giovando, J., Bartles, M., and Floyd, I. E.: Process-Based Quantification of the Role of Wildfire in Shaping Flood Frequency, *Water Resour. Res.*, 59, e2023WR035013, <https://doi.org/10.1029/2023WR035013>, 2023.
- Yu, W., Zhao, L., Fang, Q., and Hou, R.: Contributions of runoff from paved farm roads to soil erosion in karst uplands under simulated rainfall conditions, *CATENA*, 196, 104887, <https://doi.org/10.1016/j.catena.2020.104887>, 2021.
- Zaharia, L., Costache, R., Prăvălie, R., and Ioana-Toroimac, G.: Mapping flood and flooding potential indices: a methodological approach to identifying areas susceptible to flood and flooding risk. Case study: the Prahova catchment (Romania), *Front. Earth Sci.*, 11, 229–247, <https://doi.org/10.1007/s11707-017-0636-1>, 2017.
- Zakerinejad, R. and Maerker, M.: An integrated assessment of soil erosion dynamics with special emphasis on gully erosion in the Mazayjan basin, southwestern Iran, *Nat. Hazards*, 79, 25–50, <https://doi.org/10.1007/s11069-015-1700-3>, 2015.
- Zhou, Y., Liu, Y., Wu, W., and Li, N.: Integrated risk assessment of multi-hazards in China, *Nat. Hazards*, 78, 257–280, <https://doi.org/10.1007/s11069-015-1713-y>, 2015.